Technical Report No. 32-674

Determination of Some Physical Properties of the Atmosphere of Mars from Changes in the Doppler Signal of a Spacecraft on an Earth-Occultation Trajectory

Arvydas Kliore

Dan L. Cain
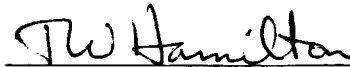
T. W. Hamilton

Technical Report No. 32-674

Determination of Some Physical Properties of the Atmosphere of Mars from Changes in the Doppler Signal of a Spacecraft on an Earth-Occultation Trajectory

Arvydas Kliore

Dan L. Cain

T. W. Hamilton

T. W. Hamilton, Chief
System Analysis Section

JET PROPULSION LABORATORY
CALIFORNIA INSTITUTE OF TECHNOLOGY
PASADENA, CALIFORNIA

October 15, 1964

CONTENTS

TABLES

FIGURES

FIGURES (Cont'd)

FIGURES (Cont'd)

ABSTRACT

$3 3 0 0 0$

The physical properties of the atmosphere of Mars are of great interest not only to astronomers, but also to the technologists who are planning to land instrumented spacecraft on the surface of the planet.

This undertaking requires an improved knowledge of both the density of the atmosphere of Mars at the surface and its variation with altitude.

This Report describes an experiment designed to achieve this objective by observing the frequency changes of the spacecraft tracking signal caused by traveling through the atmosphere of Mars prior to occultation by the planet.

The expressions describing the effects of refraction in the atmosphere are derived and used to compute expected doppler changes for several isothermal model atmospheres of Mars, using typical 1964 and 1966-67 Earth-occulting Mars fly-by trajectories. Based on these computed results, and on the expected data accuracy, it is estimated that the scale height and surface density of the atmosphere of Mars can be determined with an accuracy of better than 10% by means of the experiment.

In addition, several limitations of the experiment are described, and their effects on the results are discussed.

I. INTRODUCTION

The design of survivable lander missions to perform biological exploration of the surface of Mars requires an accurate knowledge of the physical properties of the Martian atmosphere. In particular, the surface barometric pressure must be known accurately for the design of descent parachutes, and the scale height must be known for the design of capsule structure to withstand aerodynamic heating and deceleration forces.

The present knowledge of the surface pressure on Mars is uncertain, and this uncertainty is likely to per-

sist until observations can be made with space probes. From the earlier estimates of about 85 millibars (mb), obtained by observation of Rayleigh scattering, the accepted value of the surface pressure has recently been reduced to about 10-25 mb as a result of spectroscopic investigation of CO_2 absorption bands during the last Mars opposition (Ref. 1, 2).

The knowledge of the scale height is even more fragmentary in that no direct determination can be made and that estimates are based entirely on guesses of the

temperature and constituent gases in the atmosphere of Mars.

Thus, there exists a real need for an accurate determination of the scale height and surface pressure in the atmosphere of Mars. Because direct determination with an entry capsule does not seem likely to occur in time to be useful in the design of a survivable lander for the 1969 opportunity, other means must be found to improve the knowledge of the scale height and surface pressure.

A novel approach to the problem of analyzing the structure of the atmosphere of Mars by making use of spacecraft on fly-by Earth-occultation trajectories has recently attracted considerable interest. The use of Earth-occultation trajectories was first advanced by Dr. Von R. Eshleman of the Stanford Electronics Laboratory in connection with a proposed experiment to measure the structure of the ionosphere of Mars.

Recently, one of the co-authors of this Report suggested that the effect of atmospheric refraction on the doppler tracking signal of a spacecraft on an occultation trajectory could be observed at the Earth with great precision and could be used to estimate the scale height and surface pressure of the atmosphere of Mars. The precision of two-way doppler tracking that is necessary to perform these measurements has been demonstrated in the recent *Mariner* and *Ranger* flights.

The effect of atmospheric refraction upon the propagation of electromagnetic energy is well known, and techniques have been evolved to account for the refraction by the Earth's atmosphere of tracking signals arriving from space vehicles.

An analogous effect would be observed if the tracking signal were to pass through the atmosphere of a planet, as would be the case immediately prior to the occultation of a spacecraft by a target planet. This effect could be used to advantage to gain information of the physical characteristics of the atmosphere of the target planet. A particularly attractive aspect of such a scheme is the fact that no additional payload is necessary on board the spacecraft, as only the doppler tracking signal is used, together with an occultation trajectory.

In this Report, the effect of atmospheric refraction is analyzed first using simplified models of the atmosphere, and the resulting effect on the doppler tracking signal is computed for several trajectories typical of the Mars 1964 and 1966-67 opportunities. Then an estimate is made, using the results of this analysis, of the accuracy with which it would be possible to measure the effect and to compute the atmospheric parameters in question. Finally, some of the limitations and problem areas of the experiment are discussed, and their effect on the experiment is estimated.

II. DERIVATION OF THE REFRACTION EFFECT

The effect of passing through an atmosphere on a beam of electromagnetic radiation is twofold. First, because the velocity of propagation is lower in a medium having a higher index of refraction, the electromagnetic radiation is retarded and appears to have traveled through a longer distance. In the case of a tracking signal, this effect increases the apparent range of the spacecraft.

Also, as the beam traverses regions of non-uniform index of refraction, its path deviates from a straight line, and the beam is bent by some amount as it passes through

the atmosphere. While the angle of the bending cannot be directly measured, the effect introduces an increase in the apparent range which is quite considerable if occultation occurs when the spacecraft is at a distance of the order of 10,000 km or more from the planet.

Because the two range effects vary with time, the total change in the observed doppler velocity is then the sum of both effects, as shown in the following discussion.

Figure 1 is an overall view of the geometry associated with the occultation experiment. The drawing shows the

Fig. 1. Geometry of occultation

trajectory of the spacecraft near Mars in relation to the Earth-occultation region (a cone with the viewing station on Earth as the apex) for a typical Earth-occultation trajectory. The **R-T** plane is the plane normal to the direction of the incoming asymptote **S** and the vector **B** locates the aiming point of the trajectory in the **R-T** plane. The angle θ, measured from the **T**-axis, which is parallel to the ecliptic plane, denotes the location of the trajectory aiming point with respect to the Earth-occultation region (not shown in Fig. 1 for the sake of clarity).

As the spacecraft enters the Earth-occultation cone, its radio signal must traverse a path through the atmosphere of Mars and there it experiences the refraction effect that can be observed on the Earth.

In Fig. 2(a) the geometry is shown in a simplified planar representation. Because of bending in the atmosphere, the path that is actually taken by the beam is longer than the direct path to the Earth. Thus, if R_S is the distance from the target planet to the spacecraft along the Earth-planet line, then

$$R_S = R_A \cos \epsilon \qquad (1)$$

and

$$\Delta \ell = R_A - R_S = R_A (1 - \cos \epsilon)$$

for ϵ sufficiently small

$$\Delta \ell = R_A \frac{\epsilon^2}{2} \qquad (2)$$

The contribution of this effect to the change in observed doppler velocity is then

$$\delta \dot{\rho}_\ell = \frac{d}{dt} \Delta \ell \qquad (3)$$

Finally, the contribution to the change in the observed doppler velocity due to the retardation effect ΔR is

$$\delta \dot{\rho}_R = \frac{d}{dt} \Delta R \qquad (4)$$

The total change in the observed doppler velocity may then be written as

$$\delta \dot{\rho} = \delta \dot{\rho}_\ell + \delta \dot{\rho}_R = \frac{d}{dt} (\Delta \ell + \Delta R) \qquad (5)$$

Since the expressions for ϵ and ΔR can most easily be derived in terms of h, the altitude of the ray above the surface of the planet, it is convenient to write Eq. (5) as

$$\delta \dot{\rho} = \frac{d}{dh} \left[\Delta \ell(h) + \Delta R(h) \right] \frac{dh}{dt} \qquad (6)$$

The path of the probe, viewed from the Earth, passes a distance p from the center of the planet, and is shown as a dotted line in Fig. 2(b). The apparent path of the probe is different due to refraction, and it is denoted by the solid line. From the figure it can be seen that under the assumption that the bending effect occurs at one point along the ray path, at an altitude h from the surface of the planet, the following is true:

$$h = r - r_0 + R_A \epsilon (h) \qquad (7)$$

where R_A is the probe-to-planet distance, then

$$\frac{dh}{dt} = \frac{dr}{dt} + R_A \frac{d\epsilon}{dt} = \frac{dr}{dt} + R_A \frac{d\epsilon}{dh} \frac{dh}{dt} \qquad (8)$$

and therefore

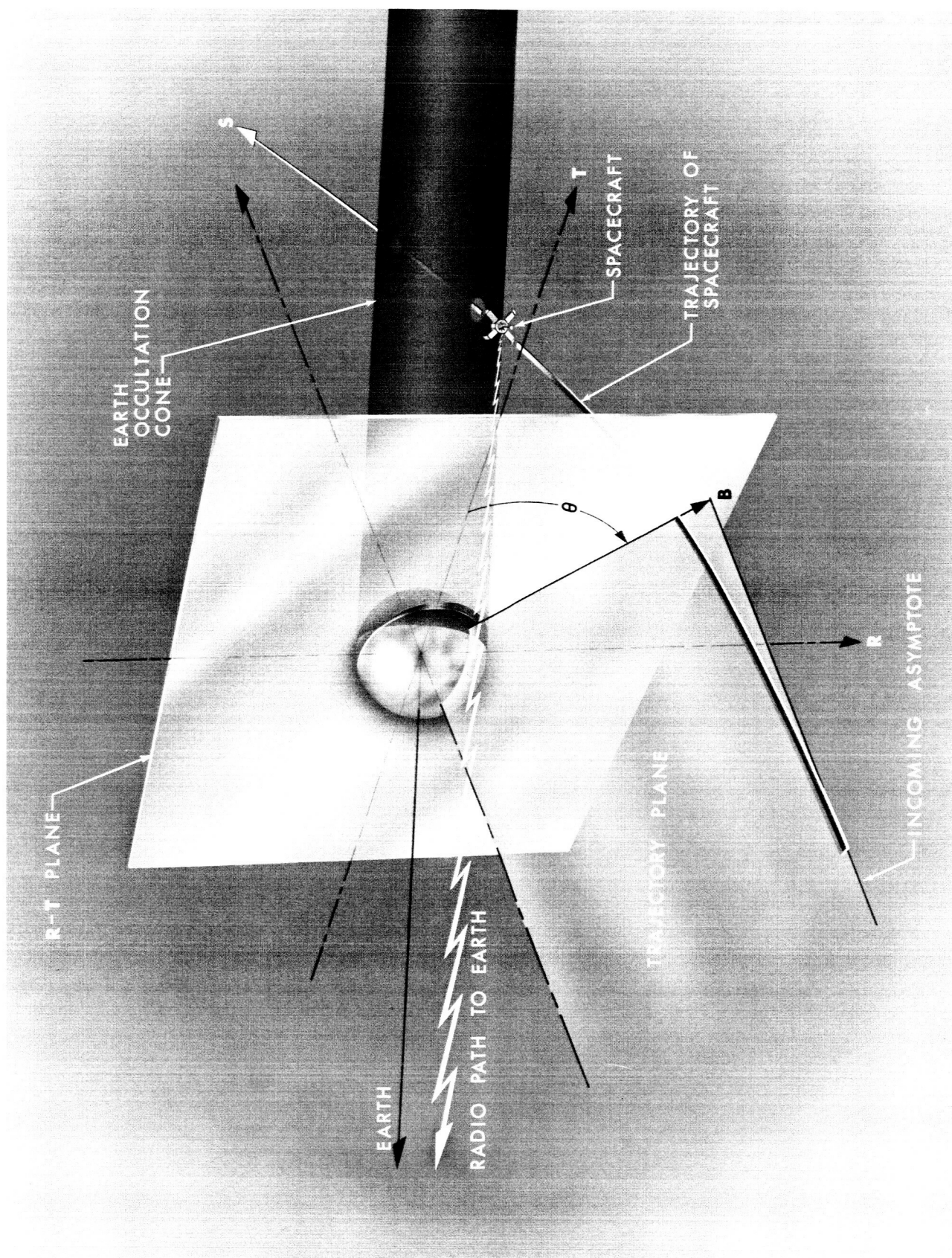$$\frac{dh}{dt} = \frac{\dfrac{dr}{dt}}{1 - R_A \dfrac{d\epsilon}{dh}} \qquad (9)$$

Fig. 2. Simplified geometry of occultation

Again, from the geometry of Fig. 2(b),

$$\frac{dr}{dt} = \frac{x}{r} \frac{dx}{dt} \tag{10}$$

but because

$$\frac{dx}{dt} = -V_{N_{pT}} = V_{N_p} - V_{N_T}$$

and

$$x = (r^2 - p^2)^{1/2}$$

Eq. (9) can be written as

$$\frac{dh}{dt} = \frac{-V_{N_{pT}} \left[1 - \left(\frac{p}{r}\right)^2 \right]^{1/2}}{1 - R_A \dfrac{d\epsilon}{dh}} \tag{11}$$

where

$$r = r_0 + h - R_A \epsilon$$

Using Eq. (11), Eq. (6) becomes

$$\delta\dot{\rho} = \frac{V_{N_{pT}} \left[1 - \left(\frac{p}{r}\right)^2 \right]^{1/2}}{1 - R_A \dfrac{d\epsilon}{dh}} \left[\frac{d}{dh} l\Delta(h) + \frac{d}{dh} \Delta R(h) \right] \tag{12}$$

The expressions for the retardation and bending effects are derived in the Appendix and are found to be approximately

$$\Delta R(h) \cong 2 \times 10^{-6} N_s e^{-\beta h} \left(\frac{\pi R}{2\beta} \right)^{1/2} \tag{13}$$

and

$$\epsilon(h) \cong \beta \, \Delta R(h) \tag{14}$$

where

$$N_s = \text{surface refractivity}$$

$$\beta = \text{inverse scale height} = 1/H$$

$$R = r_0 + h$$

and the model of the atmosphere is such that the refractivity can be assumed to be an exponential function of the altitude h, as in Eq. (15)

$$N(h) = N_s \, e^{-\beta h} \tag{15}$$

This assumption is equivalent to an isothermal atmosphere for the altitude range in question. Under these assumptions, it can be shown that (Appendix A)

$$\frac{d}{dh} \Delta R(h) = \left(-\beta + \frac{1}{2R} \right) \Delta R(h) \tag{16}$$

$$\frac{d}{dh} \epsilon(h) = \left(-\beta + \frac{1}{2R} \right) \epsilon(h) \tag{17}$$

and

$$\frac{d}{dh} \Delta l(h) = \left(-\beta + \frac{1}{2R} \right) R_A \epsilon^2(h) \tag{18}$$

Letting $k = \beta - 1/2R$ and substituting Eq. (11), (17), and (18) into Eq. (12), the following expression results for the total change in the observed doppler velocity due to refraction effects

$$\delta\dot{\rho} = \frac{k V_{N_{pT}} \left[1 - \left(\frac{p}{r}\right)^2 \right]^{1/2}}{1 + k R_A \epsilon(h)} \left[\Delta R(h) + R_A \epsilon^2(h) \right] \tag{19}$$

Since it is convenient to obtain $\delta\dot{\rho}$ as a function of time, an expression relating the altitude h to time must be found. From Eq. (11), assuming that $r_0 + h \simeq r_0$,

$$- dt = \frac{1}{V_{N_{pT}} \left[1 - \left(\frac{p}{r}\right)^2 \right]^{1/2}} \left[1 + a e^{-\beta h} \right] \tag{20}$$

where

$$a = 2 \times 10^{-6} R_A k N_s \left(\frac{\pi r_0}{2} \right)^{1/2}$$

and Eq. (20) can be integrated to give

$$\tau = \frac{1}{V_{N_{pT}} \left[1 - \left(\frac{p}{r}\right)^2 \right]^{1/2}} \left[h + \frac{a}{\beta} (1 - e^{-\beta h}) \right] \tag{21}$$

where τ is the time to occultation.

III. RESULTS FOR TYPICAL EARTH-OCCULTATION TRAJECTORIES

In order to obtain an understanding of the expected magnitude of the effect in the case of a Mars occultation, the change in doppler velocity $\delta\dot\rho$ was computed digitally using the approximate equations derived in Section II for an assumed range of hypothetical models of the atmosphere of Mars.

To implement the computations, it was necessary to obtain an estimate of the expected refractivity N_s at the surface of Mars. It is known that for the Earth's atmosphere, the value of N_s is approximately 260 at 25°C and with no water vapor present. Since the refractivity N_s varies inversely as the surface absolute temperature, T, and directly as surface barometric pressure, then, assuming that the Martian atmosphere consists mainly of nitrogen or argon, the surface refractivity for Mars can be estimated on the basis of an assumed surface pressure. At the present time, estimates of the surface barometric pressure on Mars range from 10 to 80 mb, with 25 mb accepted as most likely by some investigators. Assuming a surface temperature of 0°C, Table 1 shows the estimated values of refractivity associated with certain values of surface barometric pressure. These were used in the computation.

Table 1. Assumed values of atmospheric refractivity at the surface of Mars

Approximate % of pressure on Earth	Assumed surface barometric pressure, mb	Corresponding surface refractivity N_s
1	10	2.85
2.5	25	7.12
6.25	62.5	17.8

The expected scale height of the exponential model of the Martian atmosphere must also be assumed. Various investigators estimate the scale height near the surface to be between 5 and 20 km. In the numerical examples, three values were used, namely, 6.7, 10, and 20 km. Since three values of both surface refractivity and scale height were used, a total of nine model atmospheres result, as shown in Table 2.

The change in doppler velocity was computed for each trajectory as a function of time to occultation by a digital computer program incorporating Eq. (19) and (21) of Section II, using the nine model atmospheres

Table 2. Model atmospheres used in numerical examples

Inverse scale height β, km^{-1}	Refractivity N_s		
	2.85	7.12	17.8
0.05	1	4	7
0.1	2	5	8
0.15	3	6	9

listed in Table 2. The quantities $V_{x_{p}T}$, p, and $R_{.1}$ are computed in the program from position and velocity data extracted from the JPL Space Trajectories Program (DBH-07) at approximately the time of occultation for each of the sample trajectories.

A. Mars 1964 Trajectories

Three Mars 1964-Type I trajectories were chosen for study. The aiming points for these trajectories are shown in Fig. 3, which portrays the Earth-occultation contour
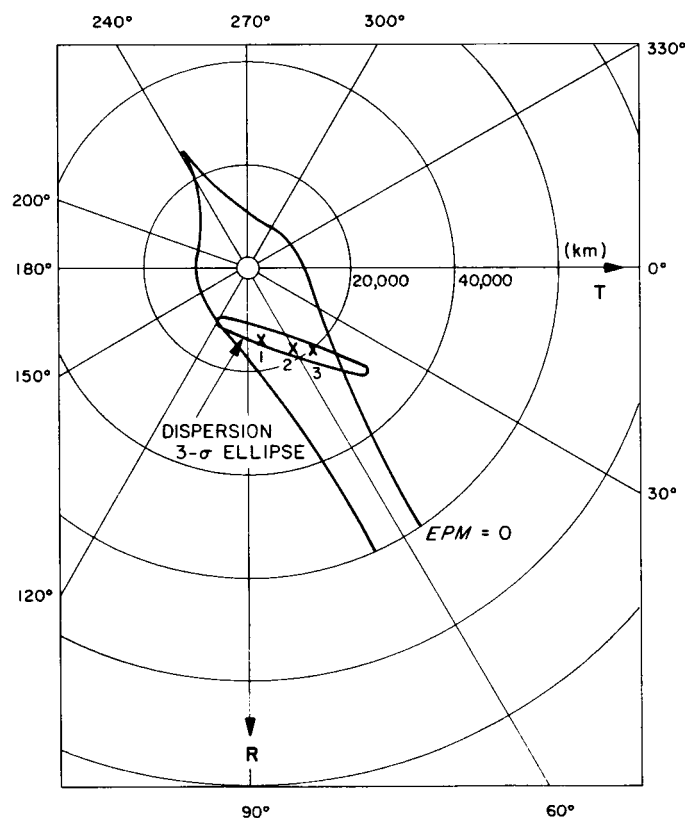

Fig. 3. R-T plane contours for typical 1964 Type I trajectories

in the **R-T** plane. All three trajectories have a November 20, 1964 launch date, and will arrive in the vicinity of Mars on July 15, 1965. The major features of the three trajectories are listed in Table 3.

Table 3. 1964 Earth-occultation trajectories[a]

Traj. No.	B, km	θ, deg	Radius of closest approach, km	Time from closest approach to start of occultation, min	Total time in occultation, min
1	18,000	60	15,780	115	60
2	20,000	50	17,780	142	55
3	15,000	80	12,890	80	48

[a] Launch date: November 20, 1964; arrival date: July 15, 1965

It can be seen from Table 3 that trajectory 1 is aimed at the center of the Earth-occultation region, while trajectories 2 and 3 are displaced from the center, but still within the 3-σ dispersion ellipse of the midcourse maneuver (assuming a 1-σ injection). A trajectory that is aimed at the center of the Earth-occultation region pierces the Earth-occultation cone through the center; and therefore, as viewed from the Earth, the distance p of Fig. 2 is zero. Trajectories not aimed at the center of the contour pierce the cone off-center and therefore p is not zero. This affects the behavior of the change in the doppler velocity as a function of time to occultation, as shown in Fig. 4–12. In addition, off-center trajectories spend less time within the occultation cone, and the total time of occultation is less, as can be seen from Table 3.

For the three 1964 Type I trajectories that are listed in Table 3, the expected change in doppler velocity (m/sec) was computed using each of the nine exponential model atmospheres of Mars. Figure 4 shows the change in doppler velocity $\delta\dot{\rho}$ as a function of time to occultation τ for trajectory 1, and the three model atmospheres having scale heights of 20 km ($\beta = 0.05$), with surface refractivities of 2.85, 7.12 and 17.8, respectively. Figures 5 and 6 show the same results for trajectory 1 and for the model atmospheres having scale heights of 10 km and 6.7 km, respectively.

Similarly, Fig. 7–9 portray the corresponding computed results for trajectory 2, and Fig. 10–12 for trajectory 3.
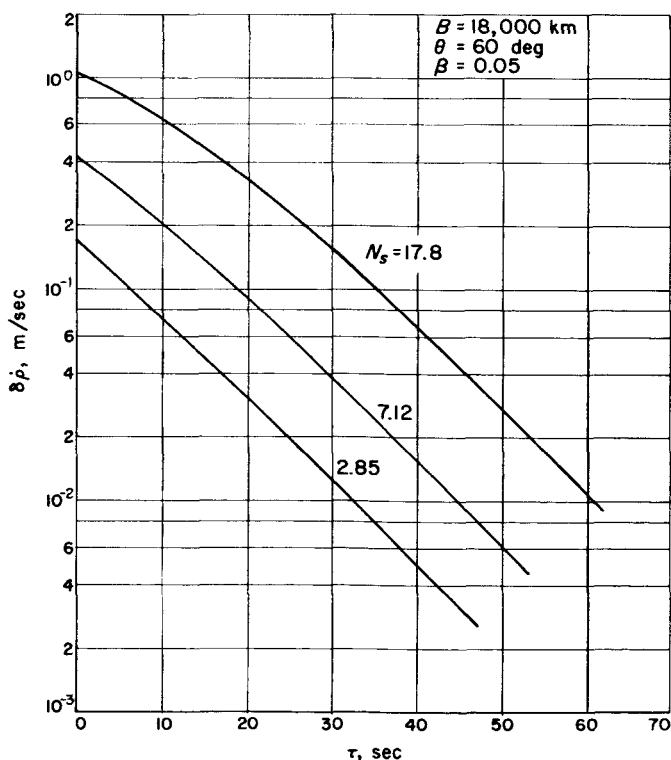

Fig. 4. Change in doppler velocity vs. time to occultation, trajectory 1, $\beta = 0.05$
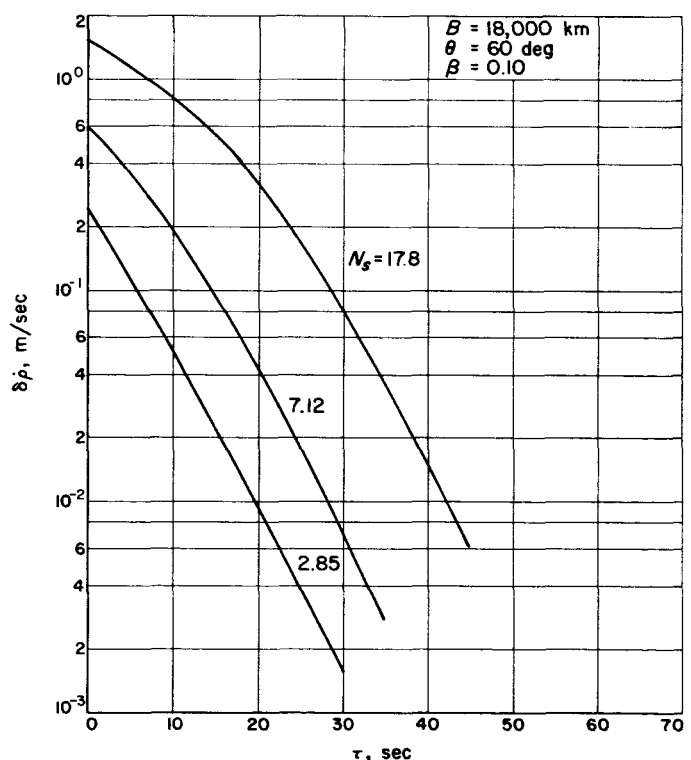

Fig. 5. Change in doppler velocity vs. time to occultation, trajectory 1, $\beta = 0.10$

Fig. 6. Change in doppler velocity vs. time to
occultation, trajectory 1, $\beta = 0.15$

Fig. 8. Change in doppler velocity vs. time to
occultation, trajectory 2, $\beta = 0.10$
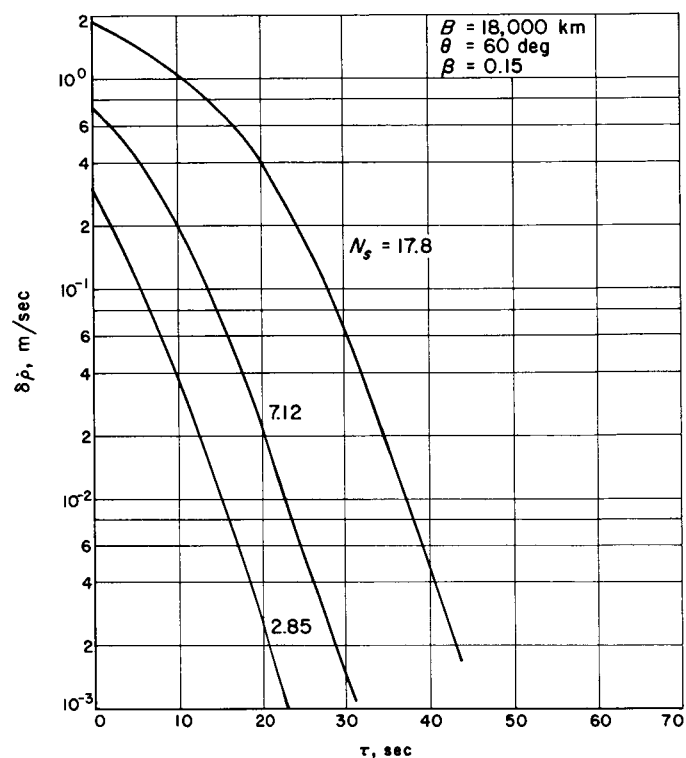

Fig. 7. Change in doppler velocity vs. time to
occultation, trajectory 2, $\beta = 0.05$
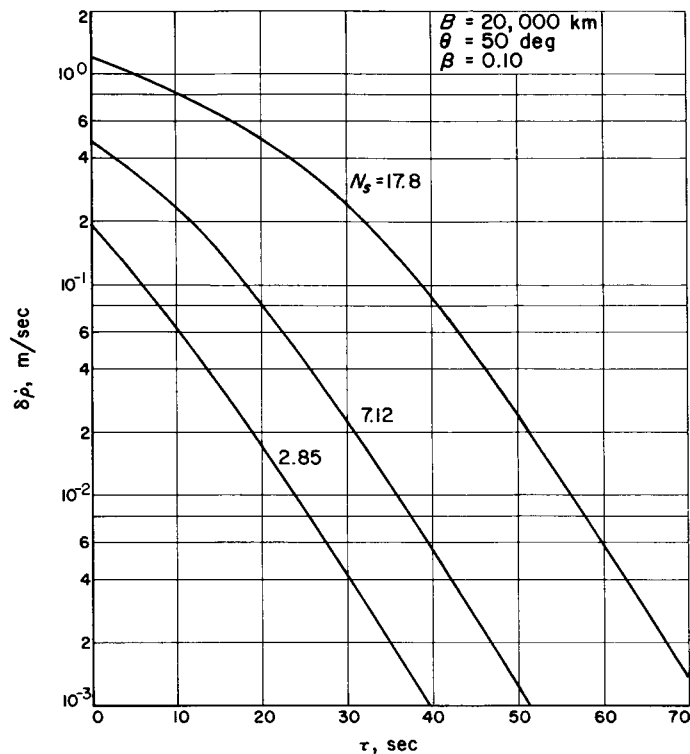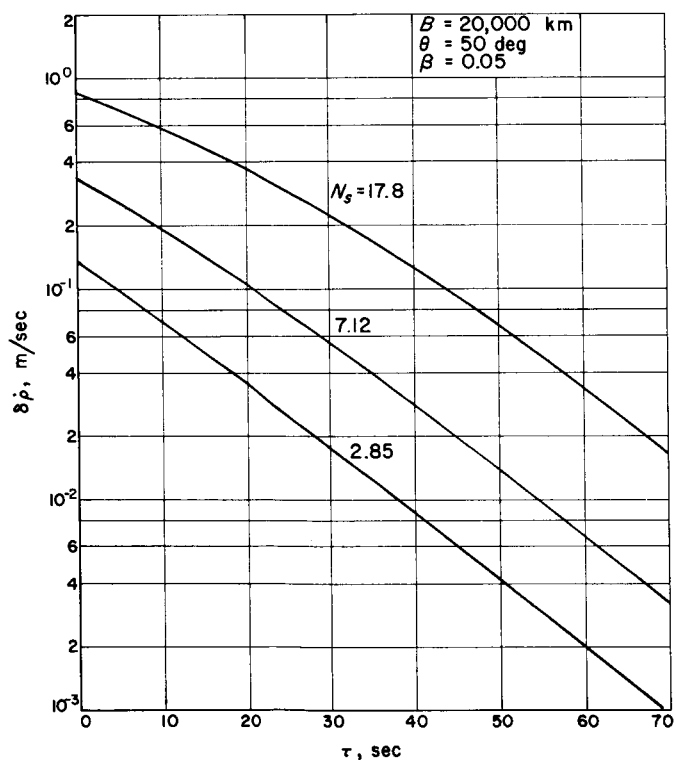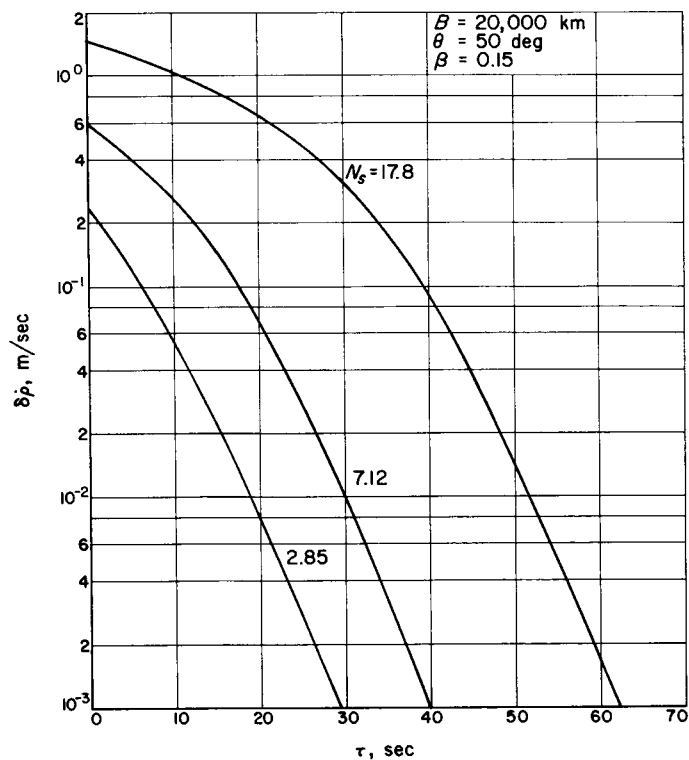

Fig. 9. Change in doppler velocity vs. time to
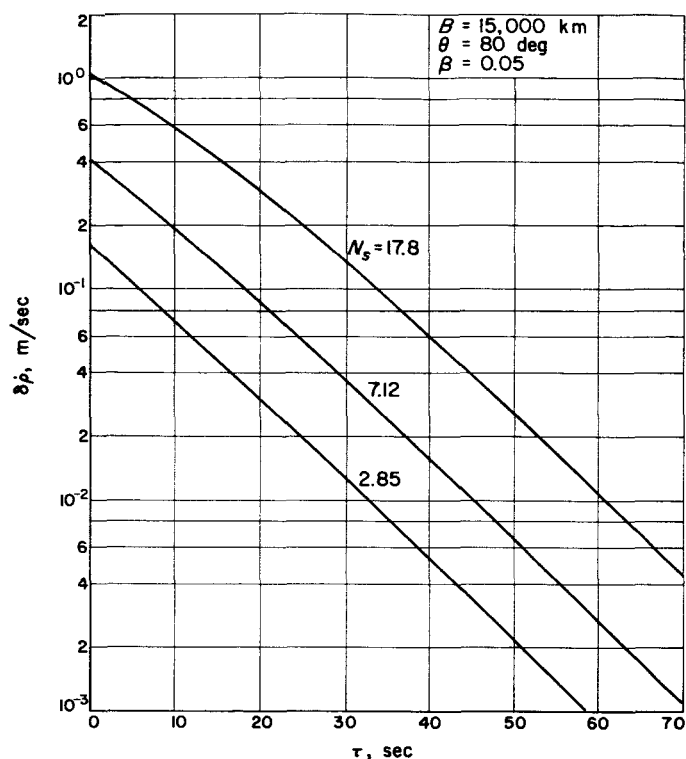occultation, trajectory 2, $\beta = 0.15$

Fig. 10. Change in doppler velocity vs. time to occultation, trajectory 3, β = 0.05
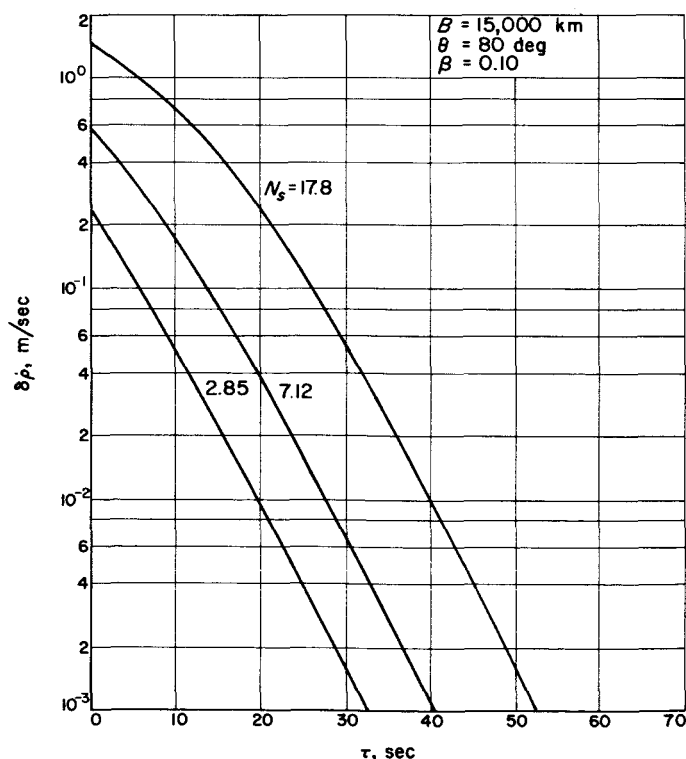

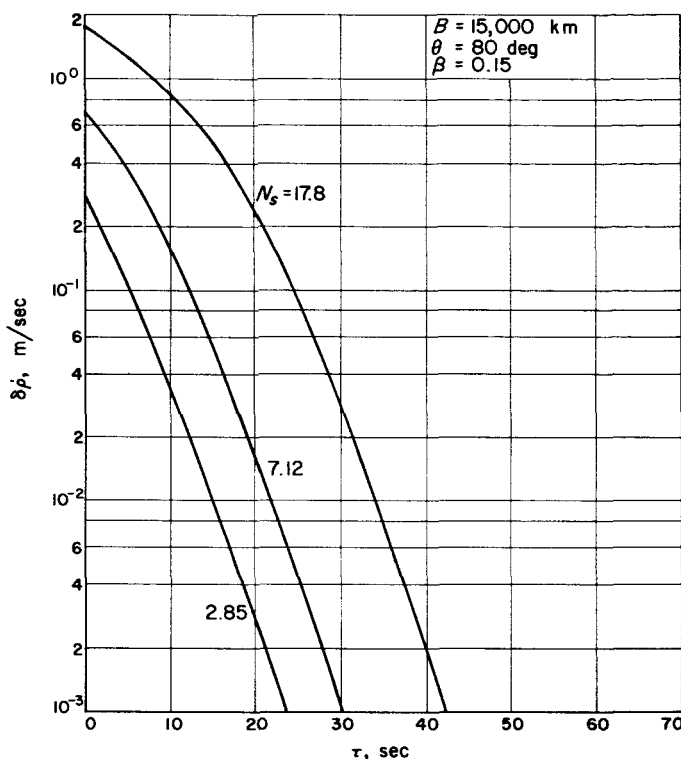**Fig. 11. Change in doppler velocity vs. time to occultation, trajectory 3, β = 0.10**

Fig. 12. Change in doppler velocity vs. time to occultation, trajectory 3, β = 0.15

Since trajectories 2 and 3 do not pass through the center of the Earth-occultation cone, the time histories of the change in doppler velocity are somewhat different than those for trajectory 1. Because of the resulting geometry difference shown in Fig. 2(b), the maximum magnitudes of the effect are somewhat reduced, and the time scale is "stretched" in the same ratio. It will be shown later that this does not materially affect the expected accuracy with which the scale height can be determined, as long as the position of the spacecraft at the time of occultation is well known.

B. Mars 1966-67 Trajectories

Three Mars 1966-67 Type I trajectories were chosen for study. Trajectories 4 and 5 correspond to a southeast launch azimuth and are to be launched about December 21, 1966, to arrive in the vicinity of Mars about July 17, 1967. The aiming points in the **R-T** plane for these two trajectories are shown in Fig. 13. Trajectory 6 results from a northeasterly launch azimuth, and corresponds to a launch date of January 27, 1967 and an arrival date of June 26, 1967.
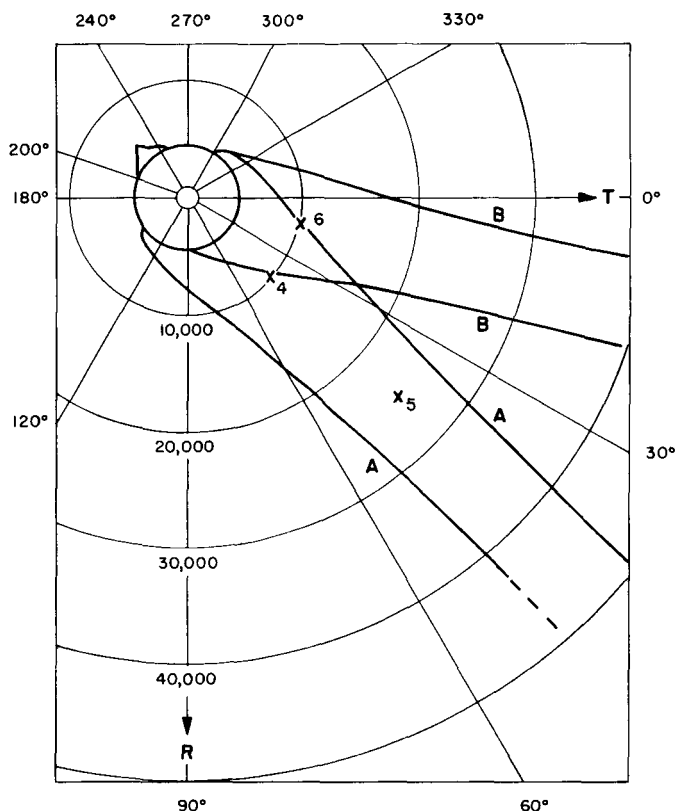
Fig. 13. Earth occultation contours in the R-T plane for typical 1966-67 trajectories

only 21 min after closest approach while trajectory 5, having a closest approach distance of 23,818 km does not enter the cone until 112 min have elapsed from the time of closest approach.

Also, because closer approach trajectories are more affected by the passage near the planet, the duration of the occultation period is shorter, as shown in the last column of Table 4.

The change in doppler velocity was computed for the 1966-67 trajectories listed in Table 4, and the results are shown in Fig. 14–22. Figure 14 shows the change in doppler velocity $\delta \dot{\rho}$ as a function of time to occultation τ for trajectory 4, and three model atmospheres having scale heights of 20 km ($\beta = 0.05$) and surface refractivities of 2.85, 7.12, and 17.8, respectively. Figures 15 and 16 show the same results for trajectory 4 and model atmospheres having scale heights of 10 km and 6.7 km, respectively.

Trajectories 4 and 5 are aimed at the center of the Earth-occultation region, as seen in Fig. 13, and differ only in the proximity of approach to the planet as determined by the magnitude of the **B** vector. It can be seen from Table 4 that because the two trajectories have widely different **B**-vector magnitudes, the times at which they enter the Earth-occultation cone are widely different. For example, trajectory 4, which has a closest approach distance of 8,908 km, enters the Earth-occultation cone

Table 4. 1966-67 Earth-occultation trajectories

Traj. No.	B, km	θ, deg	Radius of closest approach, km	Time from closest approach to start of occultation, min	Total time in occultation, min
4	10,000	45	8,908	21	31
5	25,000	45	23,818	112	40
6	10,000	14	9,298	19	25

Fig. 14. Change in doppler velocity vs. time to occultation trajectory 4, β = 0.05

Fig. 15. Change in doppler velocity vs. time to occultation, trajectory 4, $\beta = 0.10$

Fig. 17. Change in doppler velocity vs. time to occultation, trajectory 5, $\beta = 0.05$

Fig. 16. Change in doppler velocity vs. time to occultation, trajectory 4, $\beta = 0.15$

Fig. 18. Change in doppler velocity vs. time to occultation, trajectory 5, $\beta = 0.10$

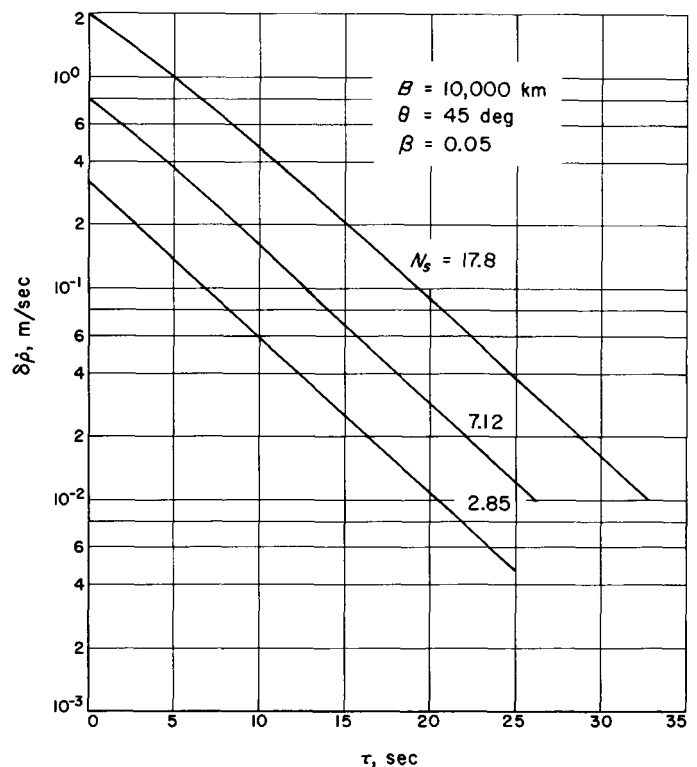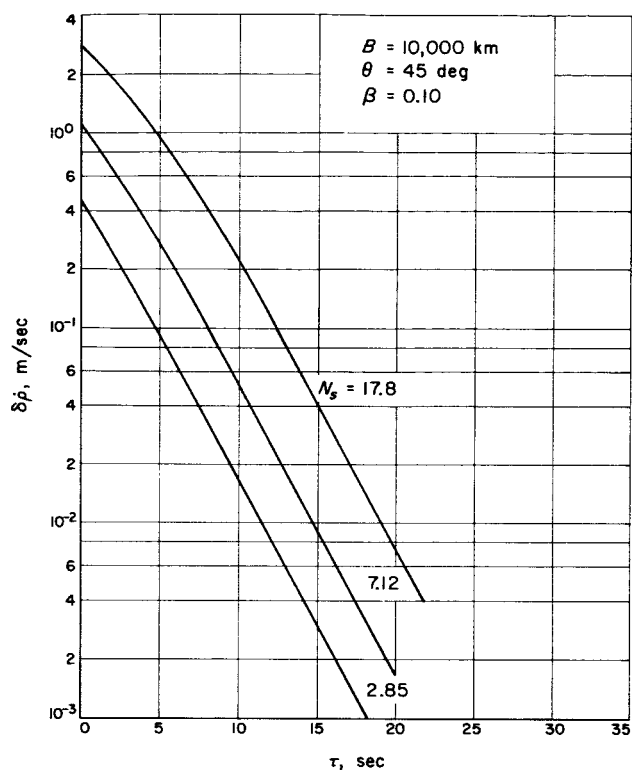**Fig. 19. Change in doppler velocity vs. time to occultation, trajectory 5, β = 0.15**

Fig. 21. Change in doppler velocity vs. time to occultation, trajectory 6, β = 0.10

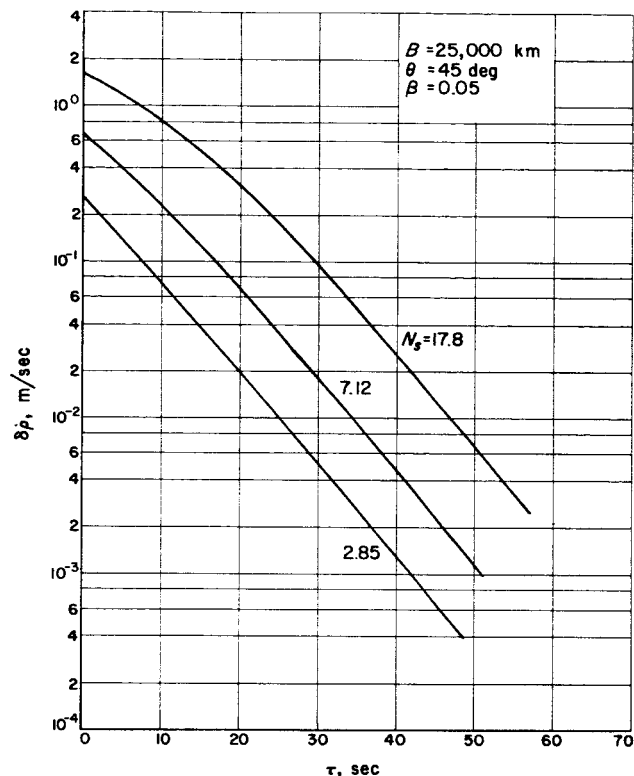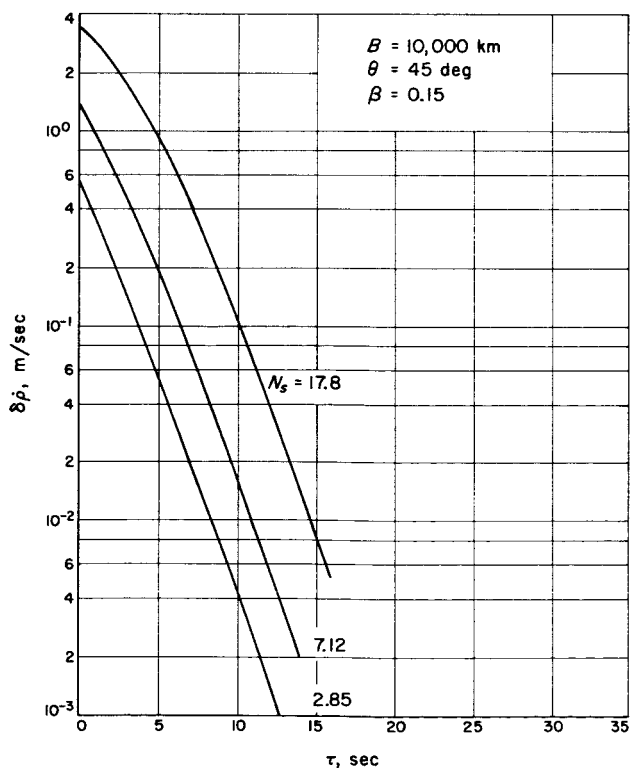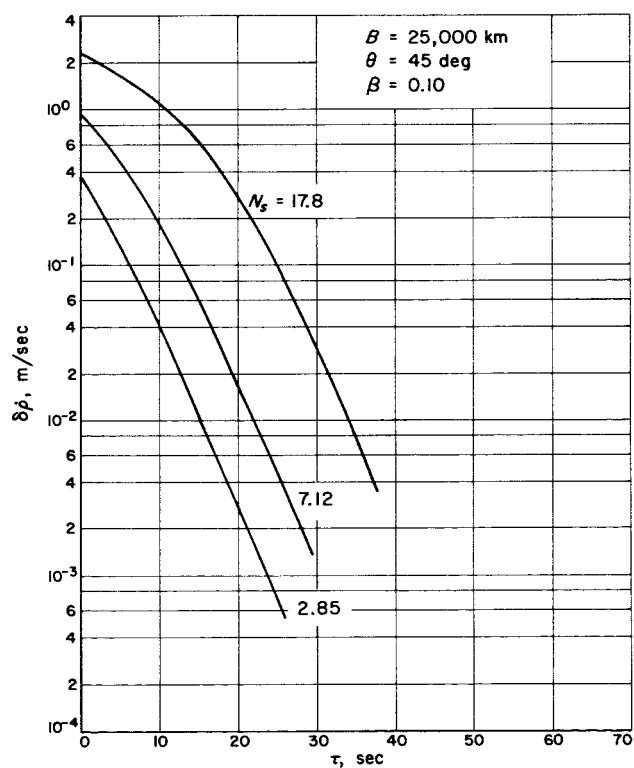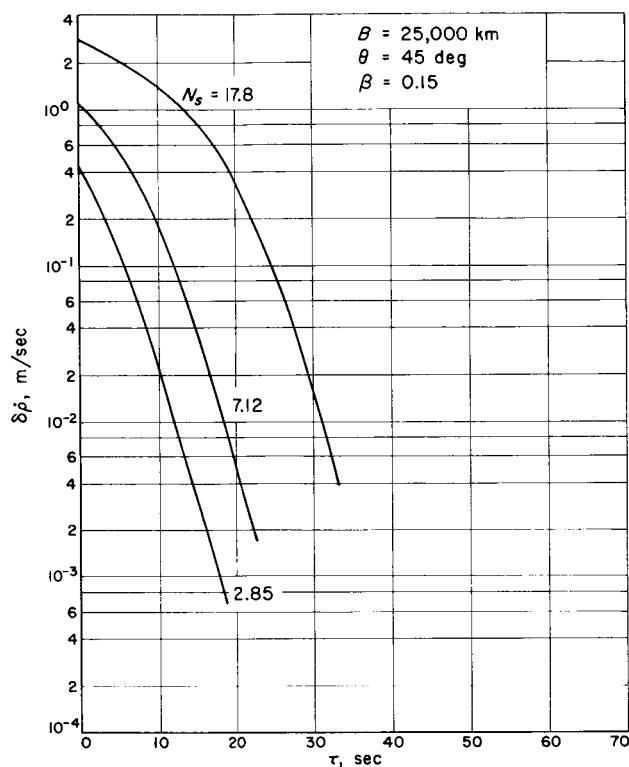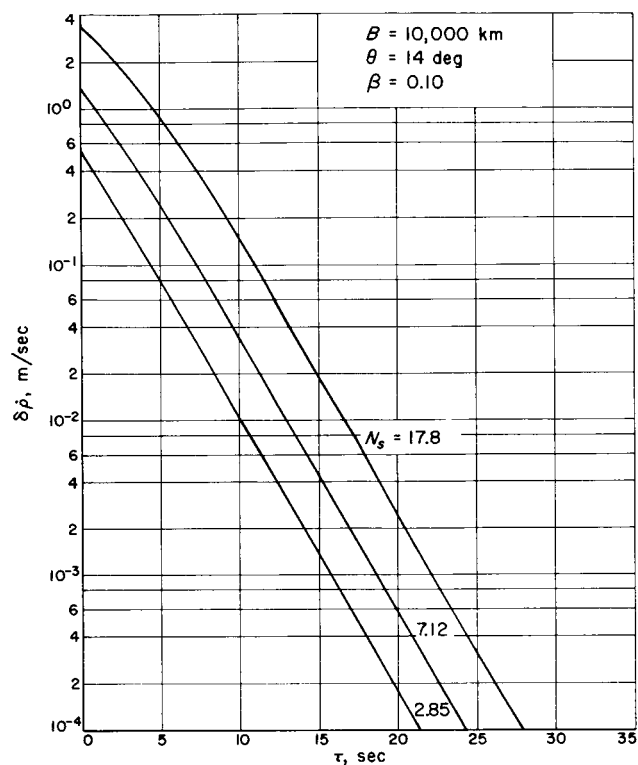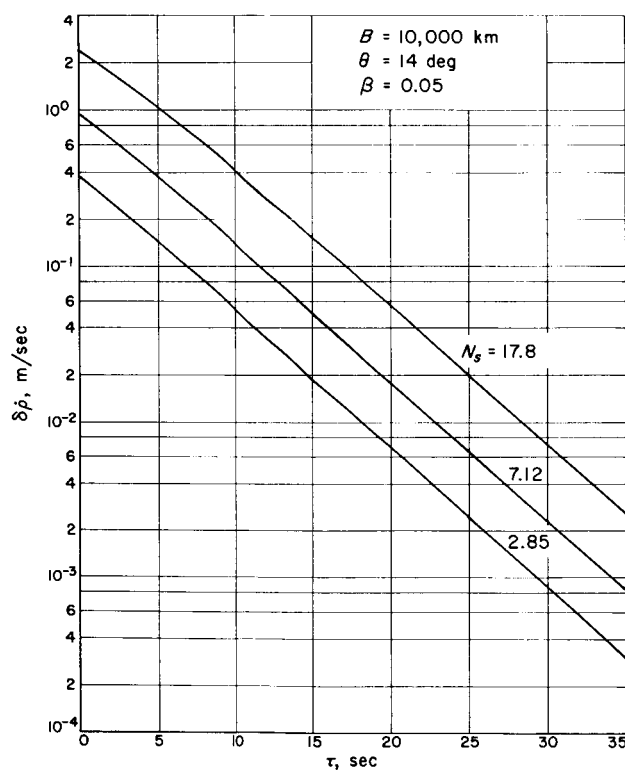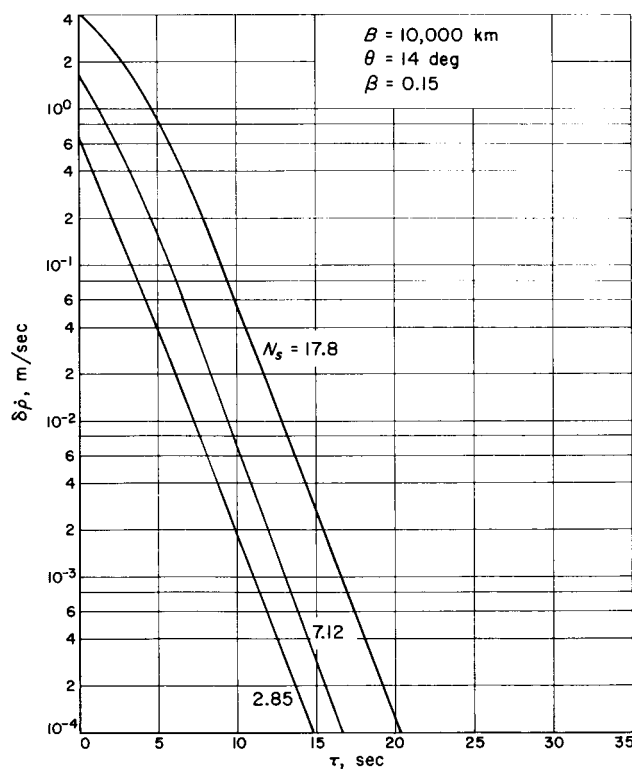**Fig. 20. Change in doppler velocity vs. time to occultation, trajectory 6, β = 0.05**

Fig. 22. Change in doppler velocity vs. time to occultation, trajectory 6, β = 0.15

Similarly Fig. 17–19 and 20–22 show the corresponding results for trajectories 5 and 6, respectively.

It may be noted that the changes in the doppler velocity corresponding to trajectory 6 have a higher maximum value and a shorter "rise time" than those corresponding to trajectory 4, which also has a **B**-parameter of 10,000 km. This arises because of the greater approach velocities inherent in the trajectories resulting from launching in the northeast direction. As will be shown later, this does not affect the accuracy of the data.

The most important conclusion that can be drawn from these results is that the expected changes in the doppler signal is well within the measurement accuracy of the Deep Space Net (DSN), even for the thinnest model atmosphere. This is further discussed in the following section.

IV. ESTIMATION OF ATMOSPHERIC PARAMETERS FROM OCCULTATION DATA

If accurate doppler were obtained during an occultation, the procedure in reducing the data would be similar to that employed in the current *Mariner* orbit determination program, which adjusts orbit, station locations, and certain physical constants simultaneously. A model would be hypothesized (at first the atmospheric model would be exactly the spherical-body, exponential atmosphere assumed here) and the data would be computed as that which would occur if the initial estimates of model parameters were true. Since this initial estimate would likely produce computed data which would not agree with the observed data, a correction to the parameters of the model would be made to yield a least-squares fit (a linearized, iterative procedure, producing better and better estimates) until no further improvement were possible. At this point judgment would be used as to the existence of systematic errors and a possible change in the model would be made at that point.

This general approach can be simplified, however, by separating the problem into two parts—at least for this preliminary analysis. It is quite probable that most of the information about the spacecraft position and velocity will come from data which are not affected by the planet atmosphere. More certainly, only data taken near occultation gives information about the planetary atmosphere. Thus, separating the data and parameters into two uncorrelated sections, the ability to observe the effects of the atmosphere on the doppler signal depends primarily on (1) the ability to predict what the doppler would be if there were no planet atmosphere or ionosphere, and (2) the ability to measure the signal received which will be affected by refraction. The difference of

(1) and (2) above is the signal which will be used to determine the atmospheric parameters. The noise, or errors, which will unavoidably arise along with the signal are depicted in Fig. 23.

A. Prediction Error

The first question is: What is the error in predicting the unaffected data? The time of the last data which are judged completely free of refraction effects is shown as t_B in Fig. 23. The error being considered now is indicated as Error 1. This is essentially the error in the prediction from data taken prior to t_B and subsequent

———— LEAST–SQUARES ESTIMATE OF NO–ATMOSPHERE DATA
————— TRUE NO–ATMOSPHERE DATA
———·—— TRUE DATA WITH ATMOSPHERE
———··—— ESTIMATE BASED ON LEAST–SQUARES FIT OF SIGNAL AND NOISE TO A MODEL
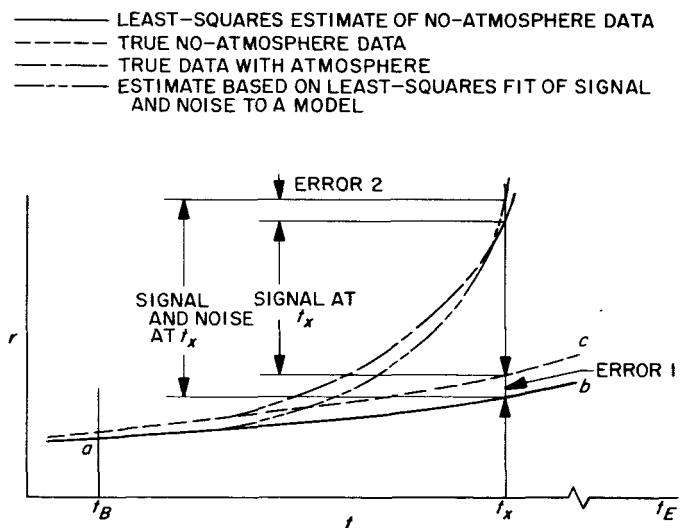

Fig. 23. Range data during occultation

to t_E (although the complete solution using the refracted data should yield a slightly better estimate).

This prediction error was analyzed briefly by means of a prediction model. The data before t_B and after t_E are used to estimate the parameters of a physical model, which are used in turn as the basis for future estimates of the doppler data (shown by the curve ac). The parameters in this model are:

1. The orbit of the spacecraft x, y, z; $\dot{x}$, $\dot{y}$ and $\dot{z}$

2. The mass of Mars

3. The astronomical unit

A typical 1966 Mars trajectory was analyzed in which the assumption was made that two-way doppler (phase-change in 1 min) data were available 10 days before and 10 days after planetary encounter. No data were taken for 10 min before and after occultation. The data were estimated to have an independent random error of 0.0125 m/sec.

The doppler data taken outside the occultation region were conservatively estimated to be 0.0125 m/sec—the data sigma now used for Ranger 6 orbit and physical constant adjustments. This figure, much larger than observed rms errors (after fitting), is used to mask solar radiation, pitch jet, antenna motions and other minor effects which would perhaps show up. Thus the weights now used in predicting cover small model errors. The variance of the orbit estimate achieved from this data (minimum variance estimate) was used to compute the variance of the estimated data taken between t_B and t_E; that is, the variance of the difference of the curves ab and ac.

Sample results from a typical case are shown in Fig. 24. The actual measurements that are to be used in the determination of atmospheric parameters are the changes-of-phase at various times; i.e., a counter is non-destructively read out. It is true that the bias, or zero set, of the counter is relatively unknown, but all the information that is needed is in the changes in the counts. This data can be represented as phase, or, after multiplying by a constant (speed of light), as range, in the following manner

$$r(t) - \dot{r}(t_0) = r(t_0)(t - t_0) + \frac{\ddot{r}(t_0)}{2}(t - t_0)^2 + \cdots \quad (22)$$

Terms of the third power in $(t - t_0)$ contribute only a very small amount relative to the data accuracy, so the uncertainties in them are insignificant. The second term,
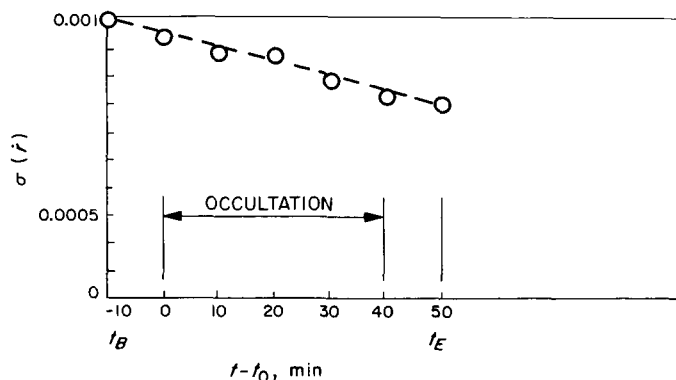

Fig 24. Range-rate prediction error

$\ddot{r}(t_0)$ does contribute significantly and an investigation of its uncertainty was made. For the case discussed above the uncertainty in $\ddot{r}(t_0)$ was 0.8×10^{-6} m/sec^2, contributing less than 1 cm phase error for $t - t_0 = 100$ sec.[1] Note that here these are the variances of the coefficients due to errors in the physical model parameters (orbit, planet mass, and astronomical unit). Therefore, the conclusion is that for two-way doppler, the uncertainty in the prediction of the phase-change during the time of occultation is approximately $0.001 \Delta t$ m (Δt in seconds). A prediction time of 1 min would yield the equivalent of about 1 cycle dropped at S-band frequency (6 cm). Of course, if the prediction time were much longer, as might be the case for larger ionospheric effects, the corresponding error would be much larger.

B. Data Accuracy

The second source of error is the error in the doppler data itself. The high-precision, two-way doppler system used by the Deep Space Instrumentation Facility (DSIF) will be briefly described. Figure 25 is an overall view of the system.

First, phase-lock assumptions are made, i.e., that:

1. The transmitter is phase-locked to the frequency standard

2. The receiver is phase-locked to the frequency standard

3. The spacecraft output is phase-locked to the incoming signal.

---

[1]For only 2 hr tracking prior to occultation, the uncertainty was 1.7×10^{-5} m/sec^2, still a small error.
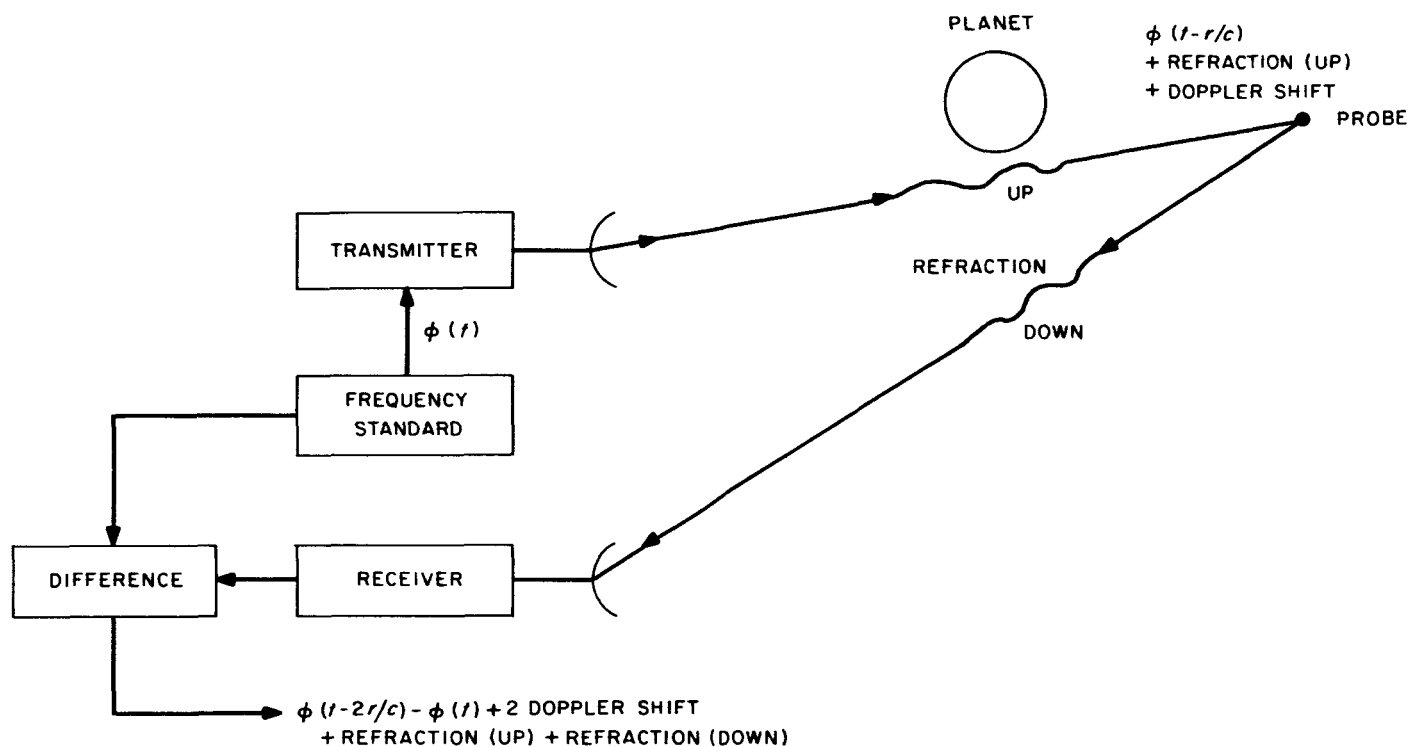
Fig. 25. Overall view of a doppler system

The precise degree to which the above is true is the subject of exhaustive effort in the area of deep space telecommunications development which has progressed over the past 10 years. The best overall judgment of the success of this effort comes from comparison of the residuals of the data (observed-minus-computed) taken from a fit to the equations of motion of the spacecraft. These observed-minus-computed values are actually the errors in cycle count divided by the count time, in order to reduce the residuals to a more comparative basis. The base frequency in the plots is 960 mc, so that 1 cps is equivalent to a range rate error of 0.156 m/sec.

Figure 26 (Mariner 2) as well as Fig. 27 and 28 (Ranger 6) are derived from the following. Figure 26 contains data taken from Mariner 2 near its encounter with Venus. Figure 27 is a portion of a pass of Goldstone data on Ranger 6 during which the crystal standard was switched off and the atomic (rubidium) standard switched on (at about 48 min from the figure reference epoch). The spacecraft was about halfway to the Moon. Figure 28 shows the last few hours before Ranger 6 impact on the Moon. The sharp rise in noise level at the end is a result of changing from a 60-sec count interval (as in Fig. 26 and 27) to a 5-sec count interval in the last few seconds before impact. The 5-sec count has a large contribution due to truncation error ($\cong \frac{1}{6}$ cps). The error

due to truncation, roundoff or "quantization" for the 60-sec data is 0.016 cps—close to the rms error in any of the plots. These plots are on observed-minus-computed values, and it should be noted that some of the noise contribution is due to the limit of 8 decimal-place computation of the computed quantities. In all, there is no evidence to date that an appreciable number of cycles is being lost or gained in any of the phase-locked circuits. Therefore, throughout this analysis, the assumption is made that the entire error is roundoff, which has a triangular distribution function, so that the rms error is $(0.038/T_c)/2^{1/2}$ m/sec, where T_c is the count time in seconds. However, the effects of extreme signal-to-noise ratios, those less than 4 db from receiver threshold, are being investigated both analytically and experimentally at present.

It was shown that a sufficient model for prediction errors is

$$r(t) - r(t_0) = \dot{r}_0(t - t_0) \tag{23}$$

There is another source of error in the measurements which is a result of the transmitter reference frequency drifting during the transit time of the signal (which is of the order of 20 min). If counting is started and continued only for a short time relative to the total transit time

GMT TIME, hr
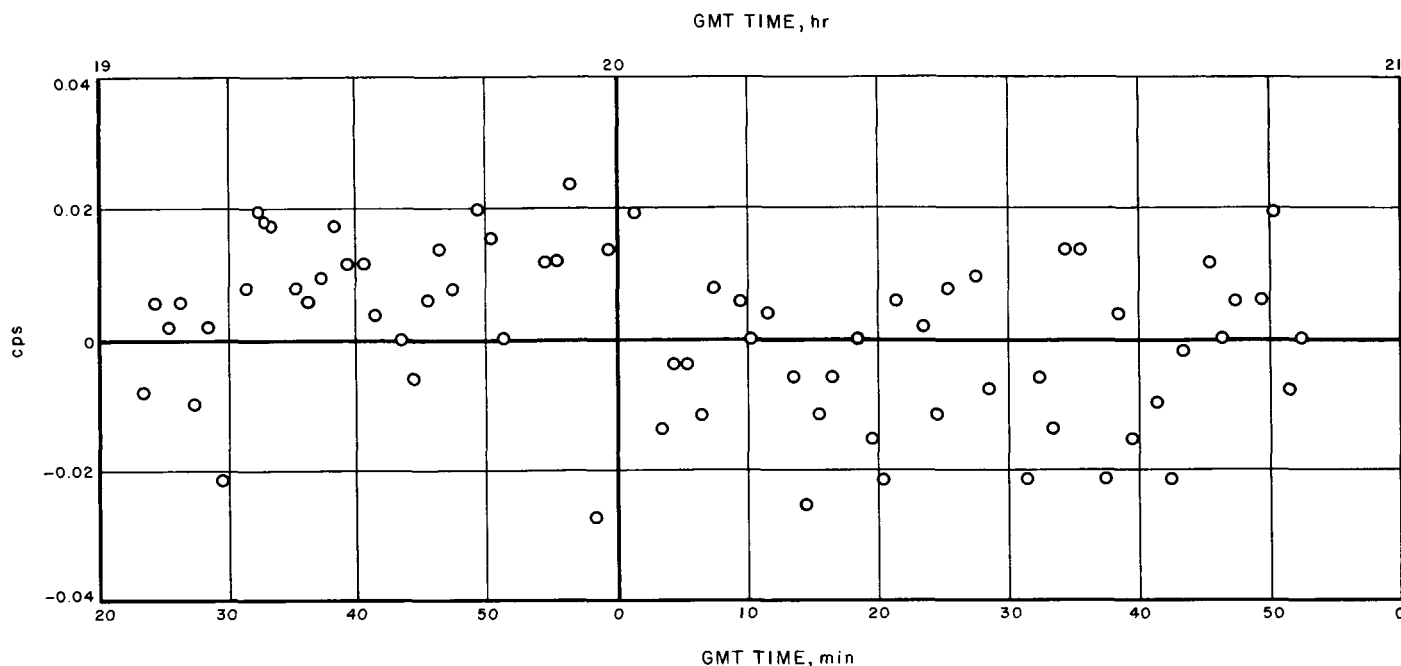
Fig. 26. Goldstone residuals, Mariner 2

(e.g., for 1 min during occultation) the reference frequency will not drift much during this short time, but will have a frequency bias and will appear just like an error in $\dot{r}_0$ of Eq. (23). It is not significant whether errors in $\dot{r}_0$ arise from physical constants or from frequency bias because $\dot{r}_0$ can be solved for using a priori data (prediction data discussed before) plus data taken during occultation.

It further can be shown, from the long-term (cruise) good fit to the *Mariner 2* data that no quadratic or higher-order error terms exist in the doppler system. Thus the model Eq. (23), is justified. If one-way doppler is used, however, the same model may not apply.

There are two or more other parameters, however, which affect data during the time of Mars atmospheric refraction; these are the scale height and the index of refraction at a reference time. A model for regression would then be

$$\delta\big[r(t) - r(t_0)\big] = (t - t_0)\,\delta\,\dot{r}_0 + \frac{\partial\,r(t)}{\partial H}\,\delta\,H + \frac{\partial\,r(t)}{\partial N_s}\,\delta\,N_s$$

$$(24)$$

where H is scale height and N_s the reference refractivity.

In this analysis the assumption has been made that $\dot{r}_0$ will be determined very well by prior data and will not affect the solution for N_s. At worst, $\dot{r}_0$ may be solved for in a common regression of $\dot{r}(t_0)$, H and N_s, with small degradation in the variances of H and N_s.

Another contribution to the data error is the frequency drift term $f(t - 2r/c) - f(t)$. Only the short-term drift of the order of minutes and less is of interest here. Research on the frequency error characteristics (Ref. 3, 4), however, (by comparing similar units) has shown this source of error to be negligible.

The figures in Table 5 below show the important results.

It is clear that in 100 sec, only part of a cycle (phase) error should result.

Table 5. Stability of frequency standards

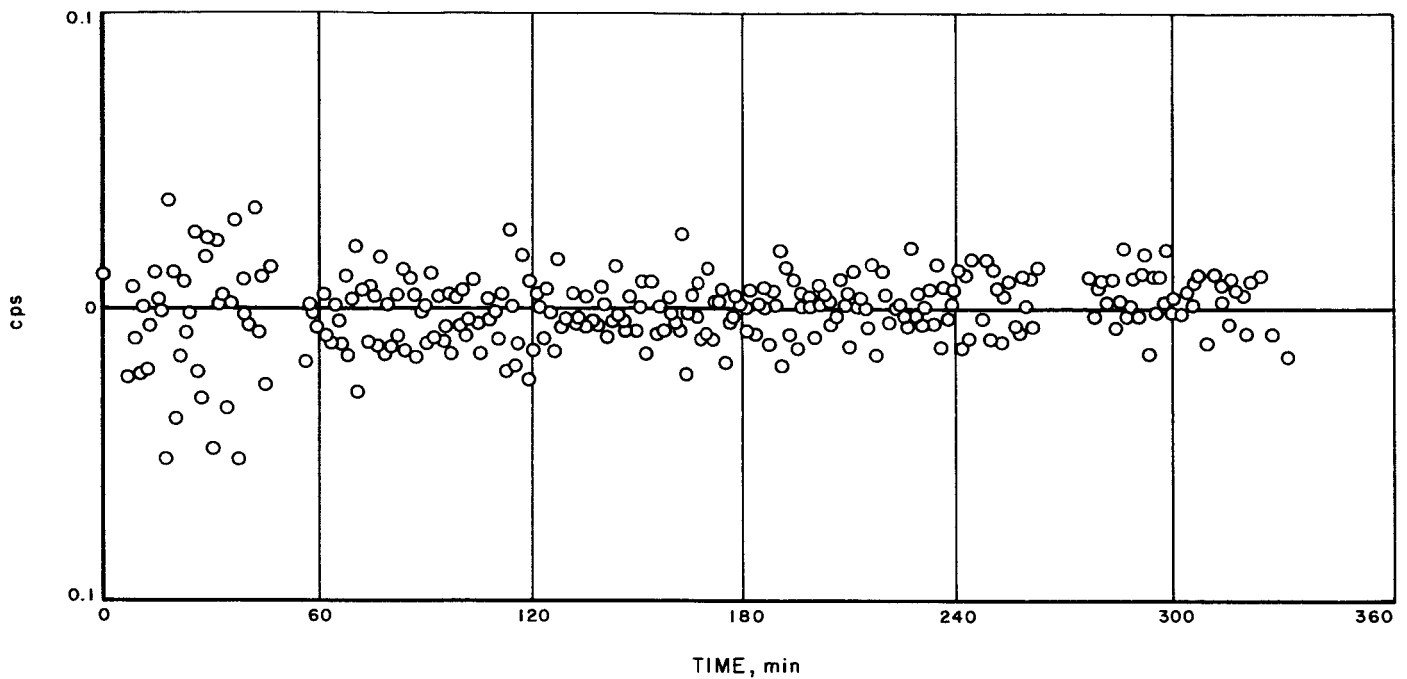| Method of measuring difference frequency	Stability-standard deviation of frequency difference divided by frequency
Measure time for 10 periods, 500 ms	2.0×10^{-11}
Measure time for 100 periods, 5 sec	0.5×10^{-11}
Digital spectrum analyzer, 40 min	0.4×10^{-11}

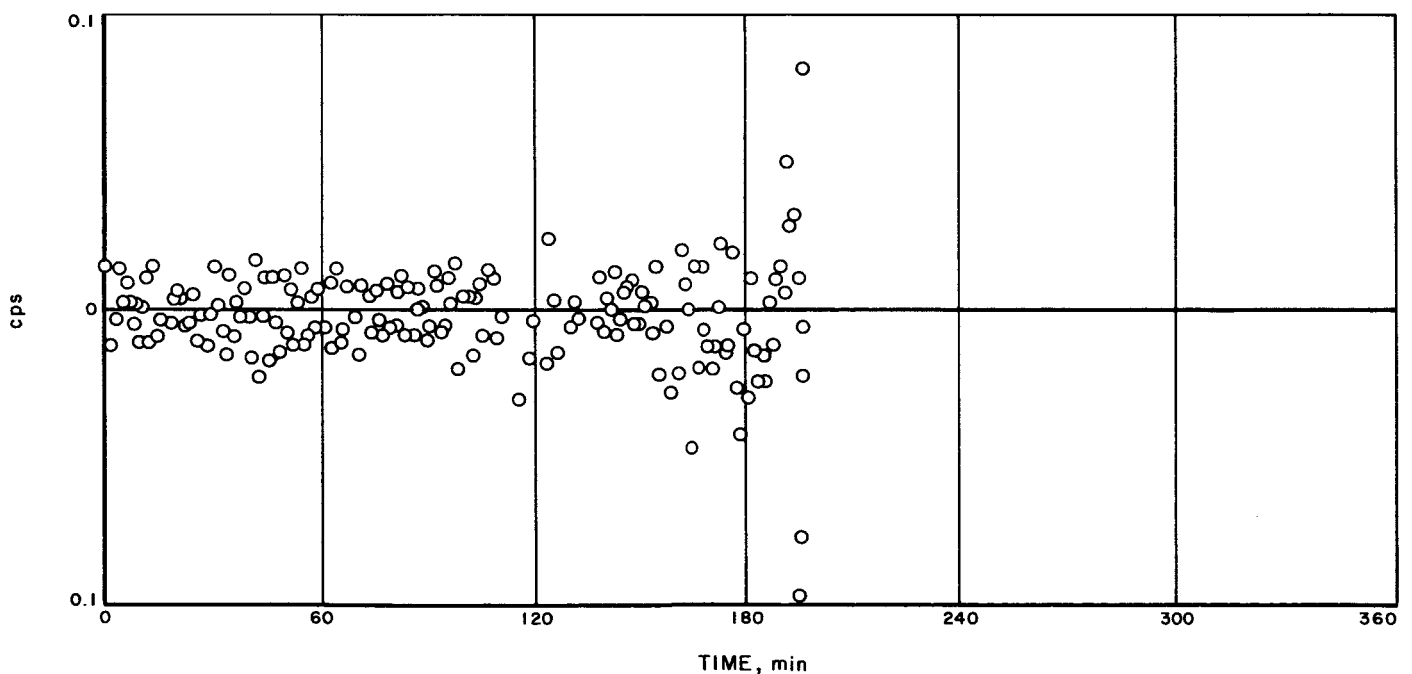**Fig. 27. Ranger 6 residuals, switching to rubidium standard at T_0**

Fig. 28. Ranger 6 residuals, switching from 60-sec count to 5-sec count at T_0

C. Simplified Accuracy Analysis

The phase-change from some zero-point has been shown to be the basic data that is expected to be taken. However, it is simpler for analysis to assume that this phase-change is only used to estimate the instantaneous range-rate. The quantity is assumed to be measured in the range rate $\dot{\rho}$ different from that predicted (negligible prediction errors assumed); and the error in this "signal" is all roundoff of standard deviation $\sigma = 0.038/T_c$.

1. Determination of Scale Height from Doppler Data

It is assumed here that the Mars atmosphere is characterized by two parameters: (1) the scale height, $H = 1/\beta$; and (2) the refractivity, N_s, at some arbitrary point in the atmosphere.

For the determination of H from tracking data as the spacecraft nears occultation by Mars, the quantities measured may be expressed as N_0 and H, where N_0 is the refractivity index near where the last data points are taken.

Note that the last data point can be determined by: (1) the surface of Mars (or irregularities); or (2) the dropout of communications as the signal margin decreases or due to failure to track the changing signal (the latter seems remote). Thus the interpretation of N_0 as the "surface" refractivity is subject to more careful examination. However, some valuable definite conclusions can be drawn regarding the minimum surface refractivity.

Consider N_0 to have a value of 2.85, 7.12 and 17.8 and examine $\beta = 0.05$ ($H = 20$ km), $\beta = 0.1$ ($H = 10$ km) and $\beta = 0.15$ ($H = 6.7$ km) with a simplified model for the variation of doppler with height, H and β. This simplification will be more accurate for low N_0 considered.

If the measurements are considered to be made at two points, 1 refers to the point associated with N_0 and 2 refers to a second point, a height Δh (known) above 1. During this period it is assumed that the measured quantity $\dot{\rho}$ varies approximately with altitude, as (Fig. 29)

$$\dot{\rho} = \dot{\rho}_0 \, e^{-\beta h} \tag{25}$$

The deterministic solution for β is then

$$\beta = \frac{\ln(\dot{\rho}_1/\dot{\rho}_2)}{\Delta h} \tag{26}$$

and therefore

$$\frac{\Delta H}{H} = -\frac{H}{\Delta h}\left(\frac{\Delta\dot{\rho}_1}{\dot{\rho}_1} - \frac{\Delta\dot{\rho}_2}{\dot{\rho}_2}\right) \tag{27}$$

Taking the variance of both sides

$$\operatorname{var}\left(\frac{\Delta H}{H}\right) = \left(\frac{H}{\Delta h}\right)^2 \left[\operatorname{var}\left(\frac{\Delta\dot{\rho}_1}{\dot{\rho}_1}\right) + \operatorname{var}\left(\frac{\Delta\dot{\rho}_2}{\dot{\rho}_2}\right)\right] \tag{28}$$
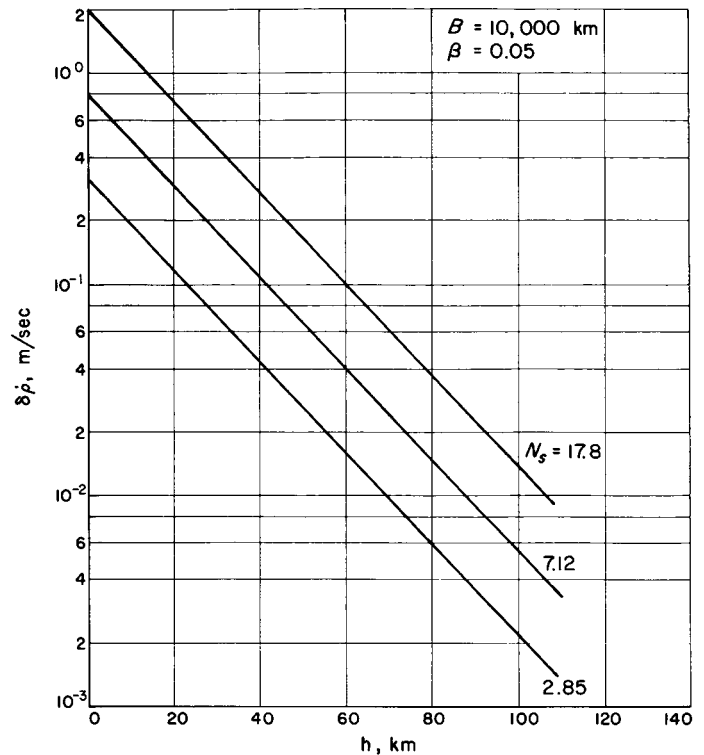

Fig. 29. Change in doppler velocity vs. altitude

and

$$\sigma\left(\frac{\Delta H}{H}\right) = \left[\operatorname{var}\left(\frac{\Delta H}{H}\right)\right]^{1/2} \tag{29}$$

The value of $\sigma\,(\Delta H/H)$ will depend on the Δh chosen and the averaging times around t_1 and t_2.

The expression in Eq. (28) was used to compute $\sigma\,(\Delta H/H)$ for each of the nine atmosphere models that are discussed in Section III, using the results shown in Fig. 4–12 for the 1964 trajectories, and Fig. 14–19 for the 1966-67 trajectories, assuming two-way doppler data. For each case, the two times t_1 and t_2 at which measurements were made and the two corresponding count times T_{c_1} and T_{c_2} were varied until $\sigma\,(\Delta H/H)$ was minimized. The results are shown in Fig. 30–34. Figure 30 shows $\sigma\,(\Delta H/H)$ as a function of the surface pressure, P_0, for three values of scale height ($\beta = 0.05$, 0.10 and 0.15) and the geometry associated with trajectory 1. Figures 31–34 show the corresponding results for trajectories 2 through 5. From Fig. 30–34 it is apparent that, even in the worst case, $\sigma\,(\Delta H/H)$ is less than 0.10, which indicates that the scale height can be determined with an accuracy of better than 10%. For an atmosphere in which the surface pressure in 25 mb (most likely estimate), the accuracy would be better than 5%.
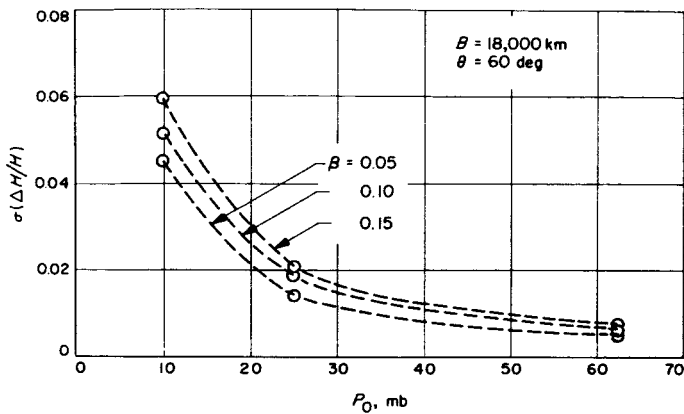
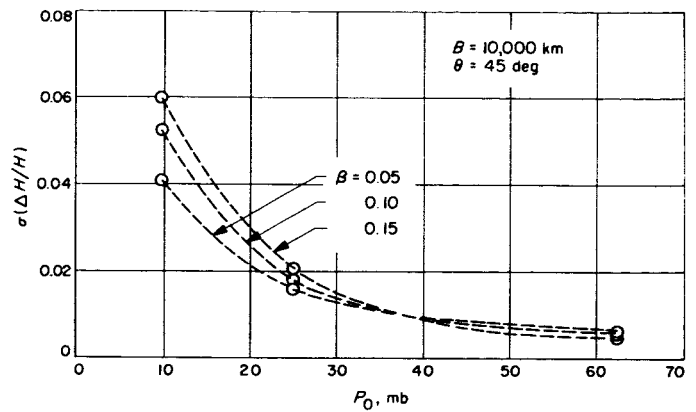**Fig. 30. Accuracy of scale height determination, trajectory 1, 1964**

Fig. 31. Accuracy of scale height determination, trajectory 2, 1964
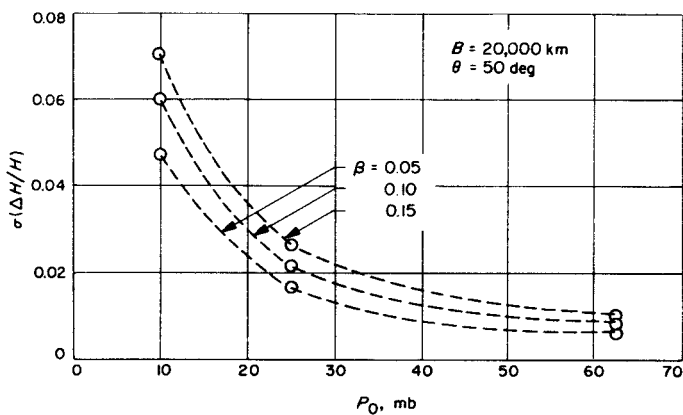

Fig. 32. Accuracy of scale height determination, trajectory 3, 1964

Fig. 33. Accuracy of scale height determination, trajectory 4, 1966-67

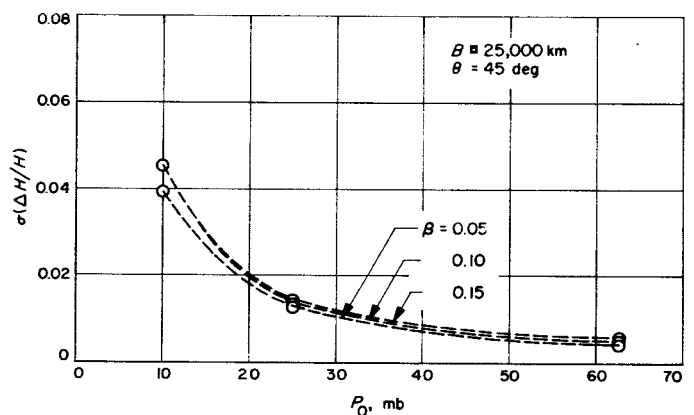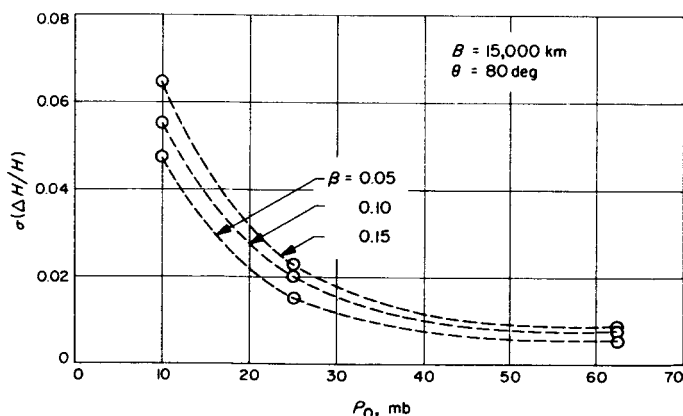**Fig. 34. Accuracy of scale height determination, trajectory 5, 1966-67**

The percent error in estimating the surface refractivity (proportional to density) can be estimated in this analysis as the percent error in measuring the range-rate change due to refraction, since this change is closely proportioned to refractivity at the reference point. It is reasonable to assume that if the signal is lost due to attenuation rather than occultation by the solid surface, the best estimation of density will come at some altitude higher than that at which the signal is lost, because the signal is large there, but also the noise due to cycle drops or adds should be proportionally greater.

For a moderate signal of 0.1 m/sec and a count time of 3 sec, the expected error is approximately 10%.

V. LIMITATIONS AND PROBLEM AREAS

In the preceding Sections, the effects arising from occultation of the spacecraft by the planet and their implications were examined from a rather idealistic point of view, taking into account only the favorable ones. However, in this as in any other phenomenon, there are also effects that are unfavorable to the observation, such as that of the attenuation of differential refraction. This effect as well as its implications are discussed here as

limitations of the experiment, together with certain other problems that may arise in connection with the experiment.

A. Signal Attenuation Due to Differential Refraction

The doppler tracking signal undergoes differential refraction as it passes through the planetary atmosphere, and, as a result, the beam is spread out and thereby attenuated. This is analogous to the effect observed in the occultation of stars by planets, except that the effect here is much less severe because of the proximity of the source.

The effect of differential refraction is analyzed in Appendix B, and the expression for the attenuation of the
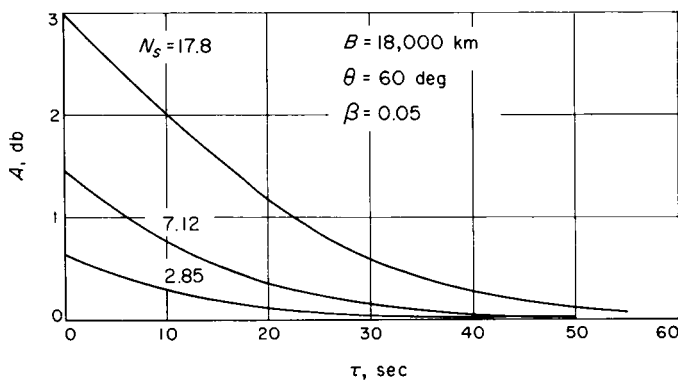
Fig. 35. Attenuation vs. time to occultation, trajectory 1, β = 0.05

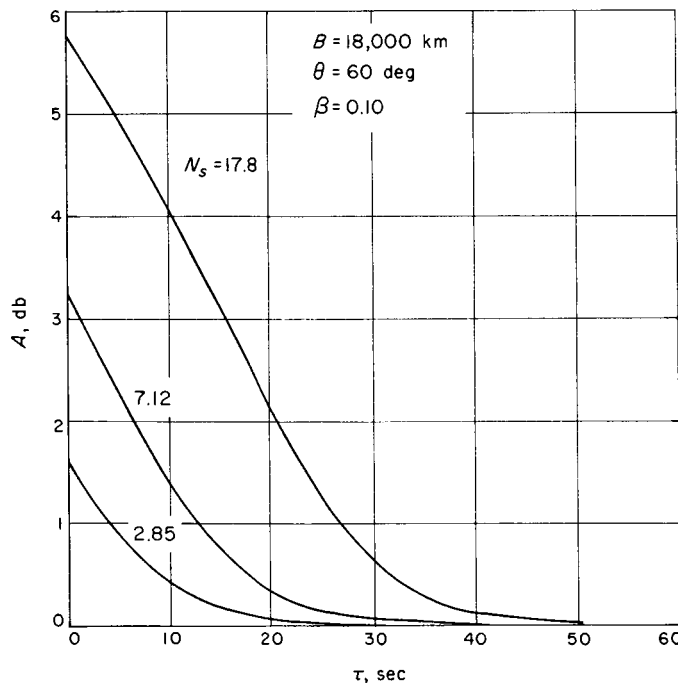Fig. 36. Attenuation vs. time to occultation, trajectory 1, β = 0.1

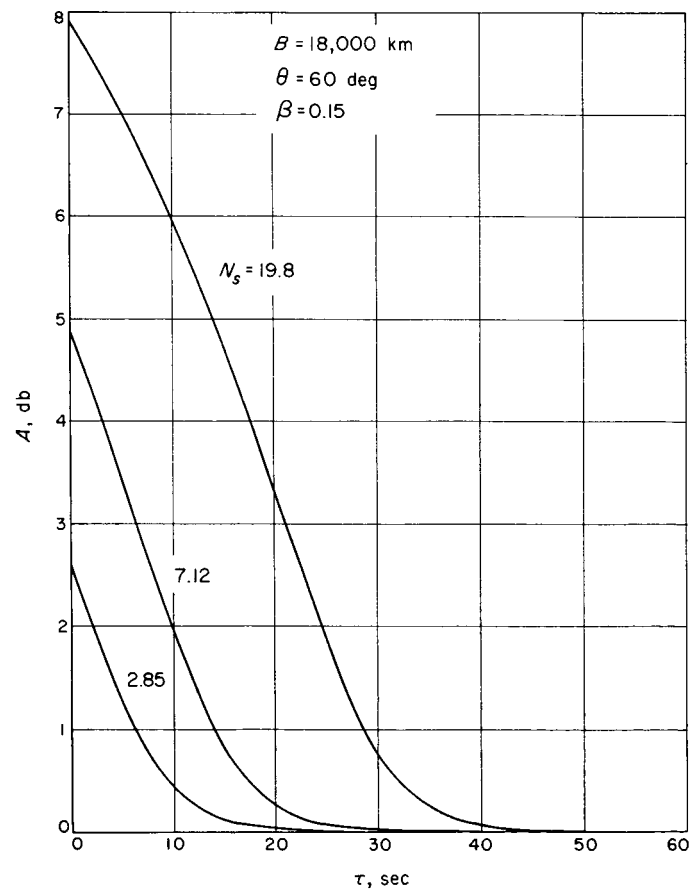Fig. 37. Attenuation vs. time to occultation, trajectory 1, β = 0.15

signal on both the "up-link" and the "down-link" is found to be

$$A(h) = 1 + \frac{R_A R_E}{R_A + R_E} \epsilon'(h) \qquad (30)$$

where

$$\epsilon'(h) = -\frac{d\,\epsilon(h)}{dh}$$

R_A = probe-to-Mars distance

R_E = Earth-to-Mars distance

Because it is true at occultation that $R_E \gg R_A$, Eq. (30) can be approximated by

$$A(h) \cong 1 + R_A \epsilon'(h) \qquad (31)$$

The attenuation effects given by Eq. (31) were computed for each of the nine models of the atmosphere of Mars that were used in Section III, and they are shown as a function of time to occultation τ, in Fig. 35–52.
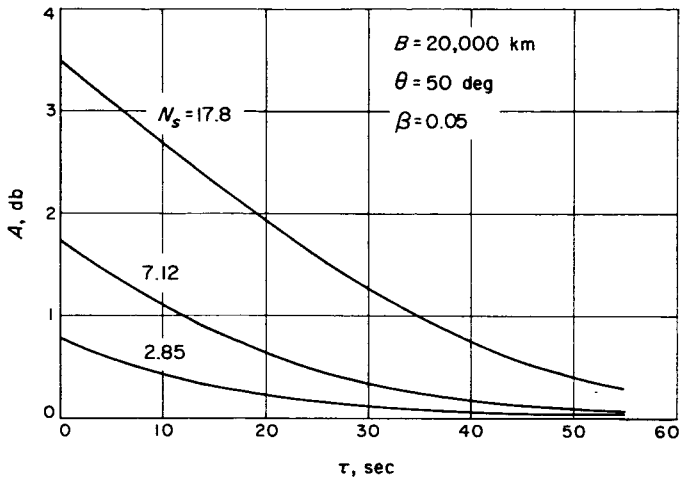

Fig. 38. Attenuation vs. time to occultation, trajectory 2, β = 0.05

Fig. 39. Attenuation vs. time to occultation, trajectory 2, β = 0.1

Fig. 40. Attenuation vs. time to occultation, trajectory 3, β = 0.15

Fig. 41. Attenuation vs. time to occultation, trajectory 3, $\beta = 0.05$
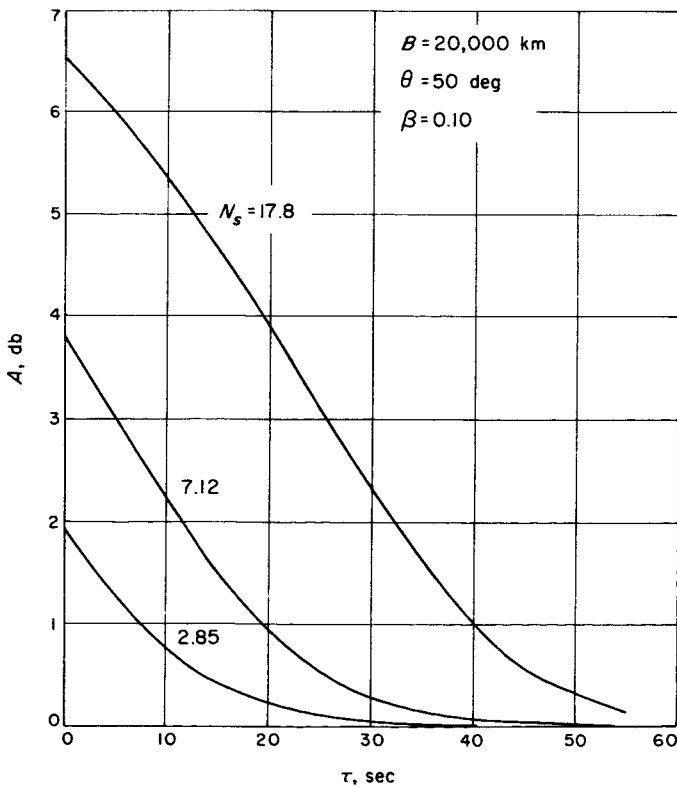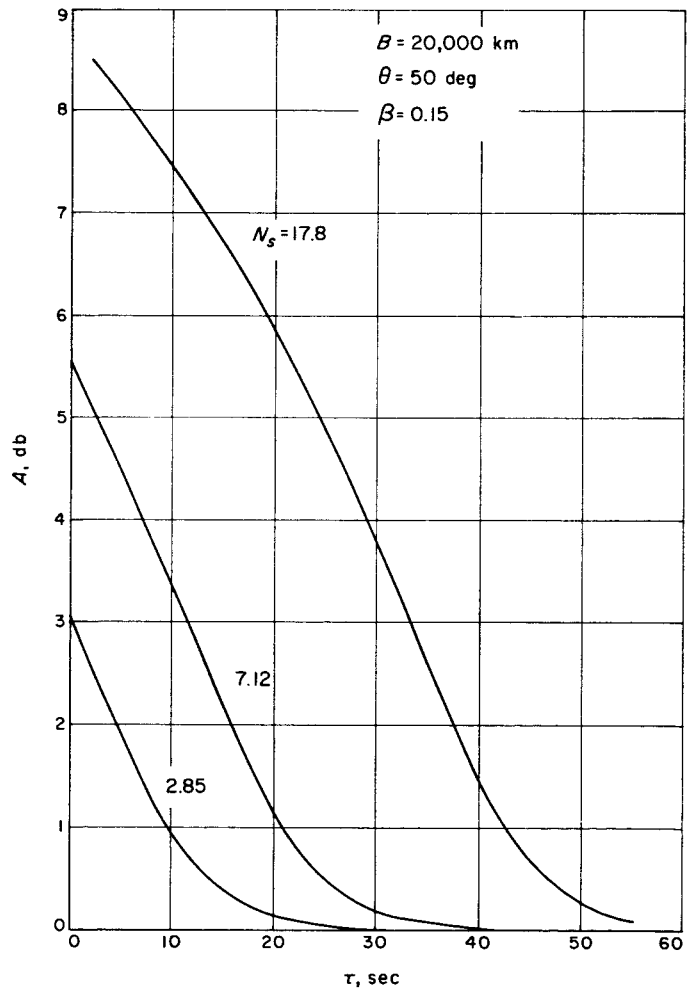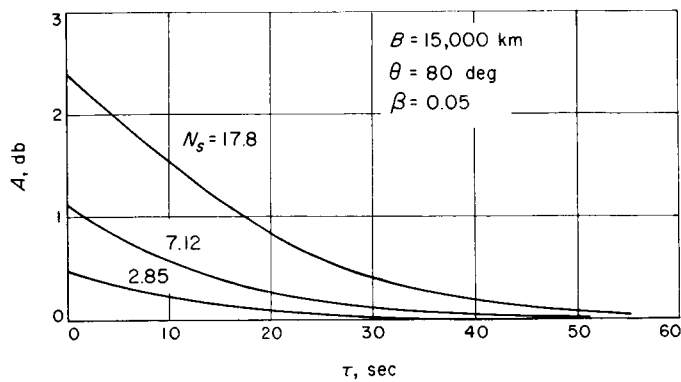

Fig. 42. Attenuation vs. time to occultation, trajectory 3, $\beta = 0.1$

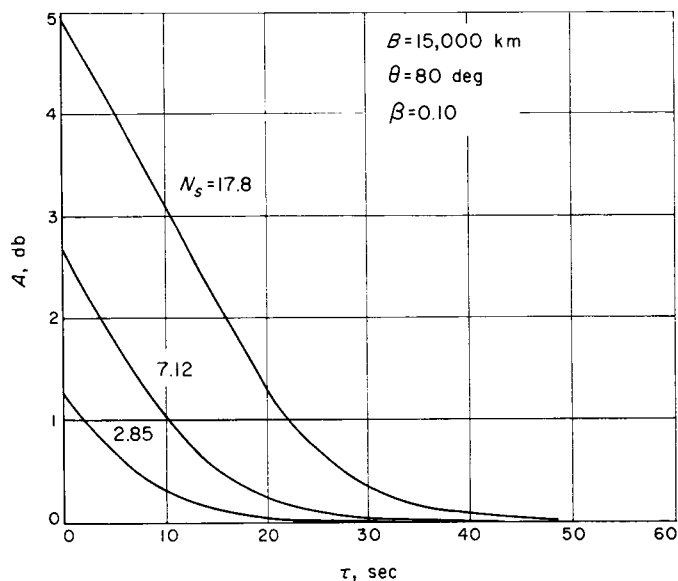**Fig. 43. Attenuation vs. time to occultation, trajectory 3, $\beta = 0.15$**
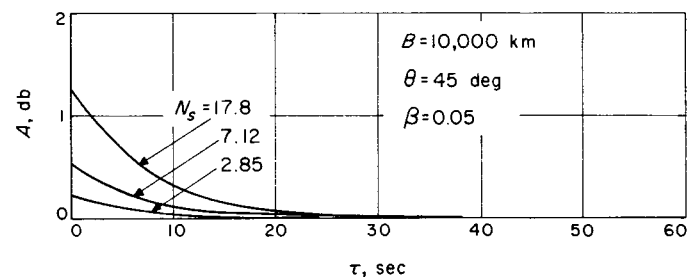
Fig. 44. Attenuation vs. time to occultation, trajectory 4, $\beta = 0.05$

Figure 35 shows the attenuation in decibels plotted for $\beta = 0.05$ and for all three values of surface refractivity, N_s, for a spacecraft on trajectory 1 of Section III. Figures 36 and 37 show plots for $\beta = 0.1$ and 0.15, respectively.

Similar results are shown for the 1964 trajectory 2 in Fig. 38–40 and for trajectory 3 in Fig. 41–43. Corresponding results for the 1966-67 trajectories 4, 5 and 6 are shown in Fig. 44–52.

It can be seen from these graphs that attenuation is strongly dependent on the values of the scale height,

surface refractivity, and the miss parameter B, which determines the distance from the planet at which occultation occurs. Whereas the attenuation at the surface is approximately 0.2 db for the most favorable conditions ($N_s = 2.85$, $\beta = 0.05$ and $B = 10,000$ km), it is approximately 9 db for the other extreme ($N_s = 17.8$, $\beta = 0.15$ and $B = 25,000$ km).

Obviously, if the parameters of the atmosphere and of the trajectory were such that the attenuation would exceed the communications performance margin of the

Fig. 45. Attenuation vs. time to occultation, trajectory 4, β = 0.1

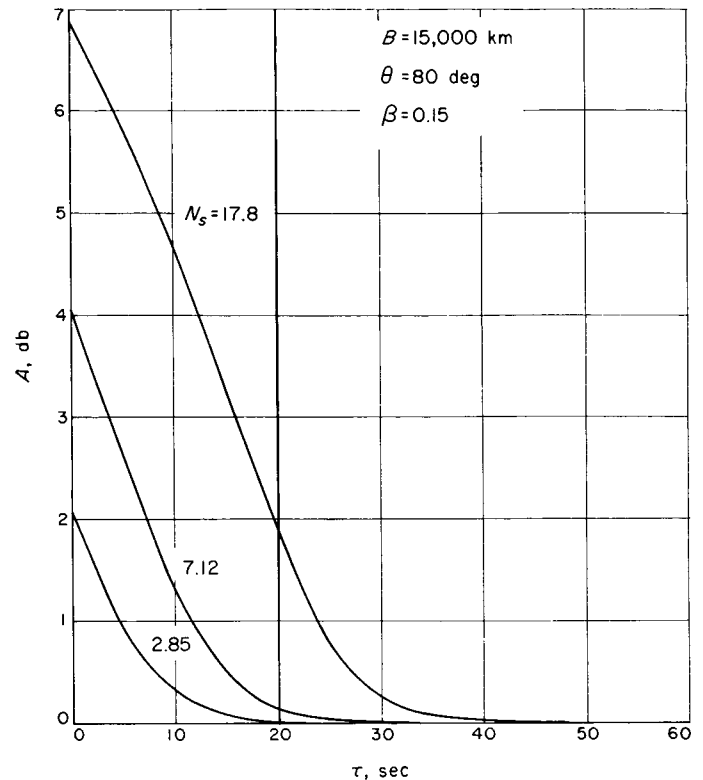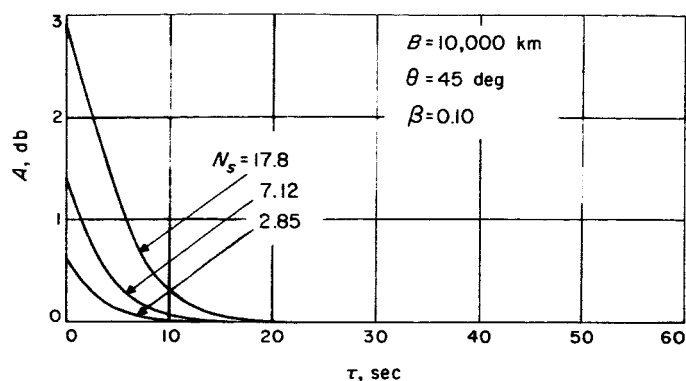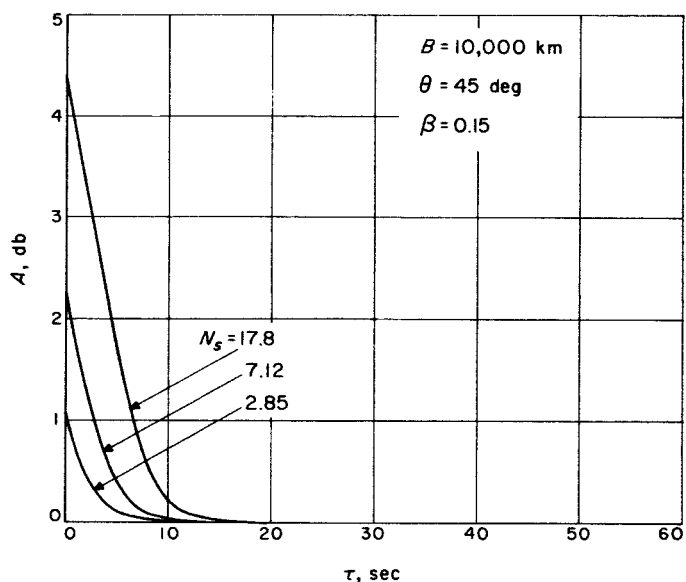**Fig. 46. Attenuation vs. time to occultation, trajectory 4, β = 0.15**

Fig. 47. Attenuation vs. time to occultation, trajectory 5, β = 0.05

Fig. 48. Attenuation vs. time to occultation, trajectory 5, β = 0.1

spacecraft, the signal would be lost before actual (physical) occultation would occur. In that case, measurements could not be made with the beam passing through all regions of the atmosphere down to the surface, but there is a limiting value of refractivity which could be measured before the signal became attenuated beyond the performance margin of the system. This limiting value of refractivity, translated to an equivalent barometric pressure, was computed as a function of the performance margin for each trajectory and four values of scale height (β = 0.05, 0.067, 0.1 and 0.15), and the results are shown in Fig. 53–58. It can readily be seen that for any value of performance margin, the limiting barometric pressure depends greatly on the scale height
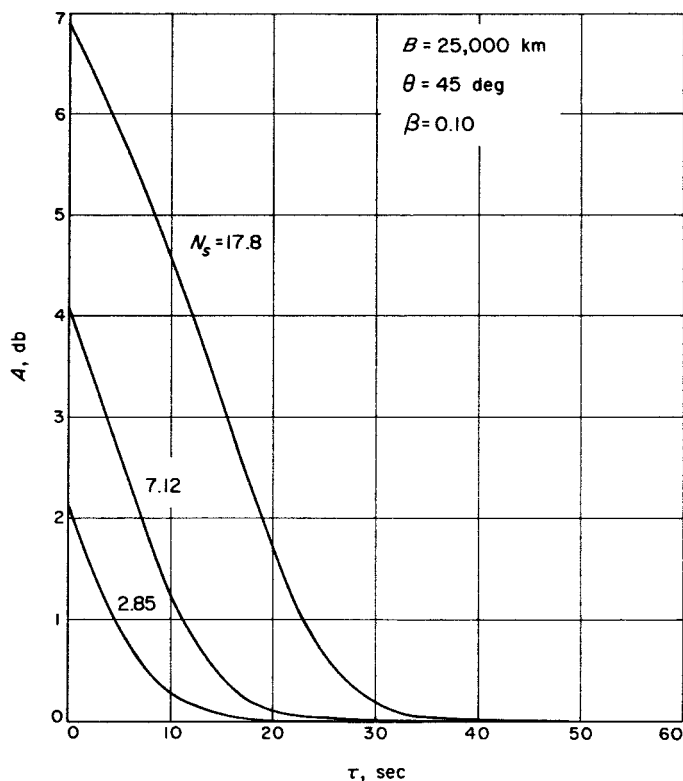
of the atmosphere. For example, a performance margin of 2 db allows the measurement of barometric pressures up to about 5 mb for β = 0.05, and 27 mb for β = 0.05 for trajectory 2 (Fig. 57). Similarly, a performance margin of 4 db, such as can be expected for *Mariner Mars*
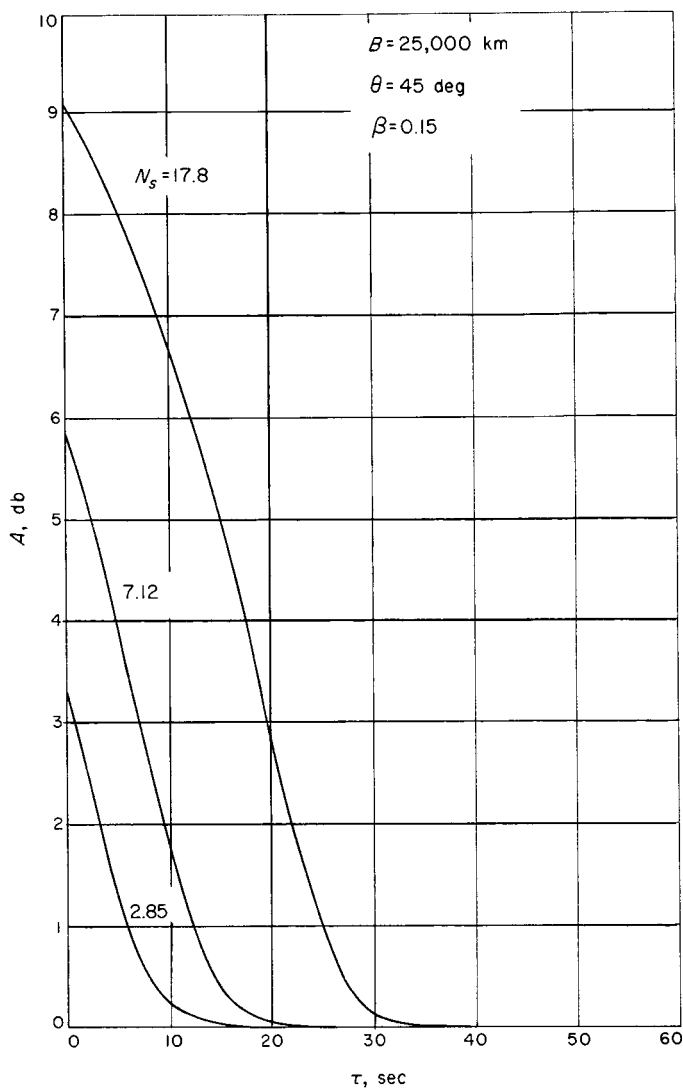
Fig. 49. Attenuation vs. time to occultation, trajectory 5, β = 0.15

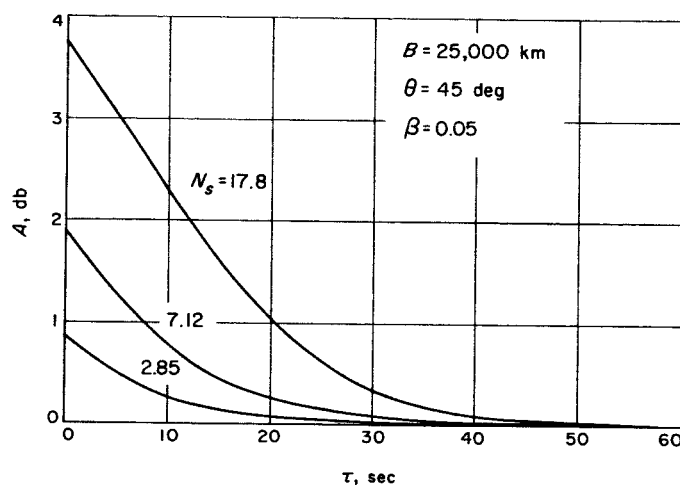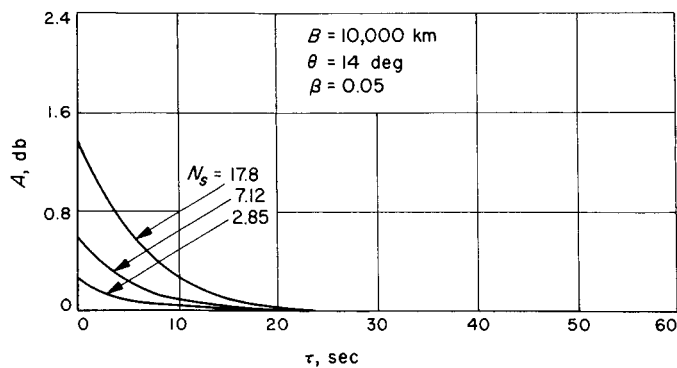**Fig. 50. Attenuation vs. time to occultation, trajectory 6, β = 0.05**
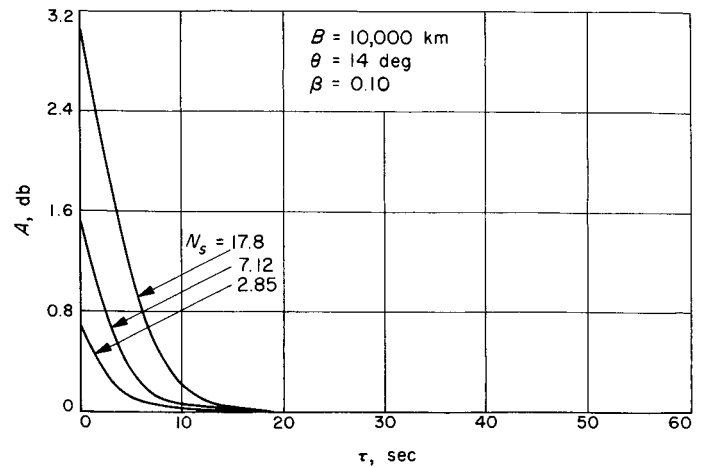
Fig. 51. Attenuation vs. time to occultation, trajectory 6, β = 0.10
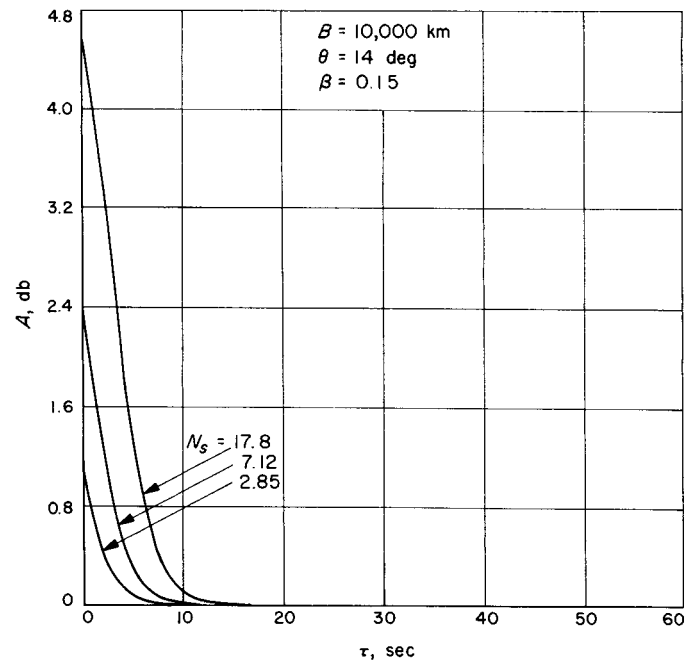
Fig. 52. Attenuation vs. time to occultation, trajectory 6, β = 0.15

1964 at encounter, allows the measurement of pressures up to a limit of 18 to over 95 mb, depending on the scale height of the atmosphere and on the trajectory, as shown in Fig. 53.

In summary, it is clear that under certain conditions, i.e., a low scale height and high value of surface barometric pressure in conjunction with a low communications performance margin, it is possible to lose signal because of attenuation due to differential refraction before actual occultation.

Fig. 53. Maximum measurable pressure vs. communications performance margin, trajectory 1, 1964

Fig. 55. Maximum measurable pressure vs. communications performance margin, trajectory 3, 1964

Fig. 54. Maximum measurable pressure vs. communications performance margin, trajectory 2, 1964

However, such cases may be distinguishable from actual occultations because in the latter case the behavior of the signal strength before extinction would be different. In any case, a lower limit for the value of surface refractivity would be established by taking data until the signal is extinguished by attenuation.

Finally, it should be pointed out that because of Fresnel diffraction at the limb of the planet, the attenuation curves shown in Fig. 35–52 should show a fluctuation near the time of occultation. This fluctuation would have a period of about 1 cps and a peak magnitude of up to 1 db.

B. Multipath Effects

Another degrading effect that must be considered is the effect of signals reflected to the Earth from the surface of the planet. Such signals, if their intensity were comparable to the intensity of the signal arriving directly from the spacecraft, would cause discrimination problems. The approximate geometry of the problem is shown in Fig. 59.
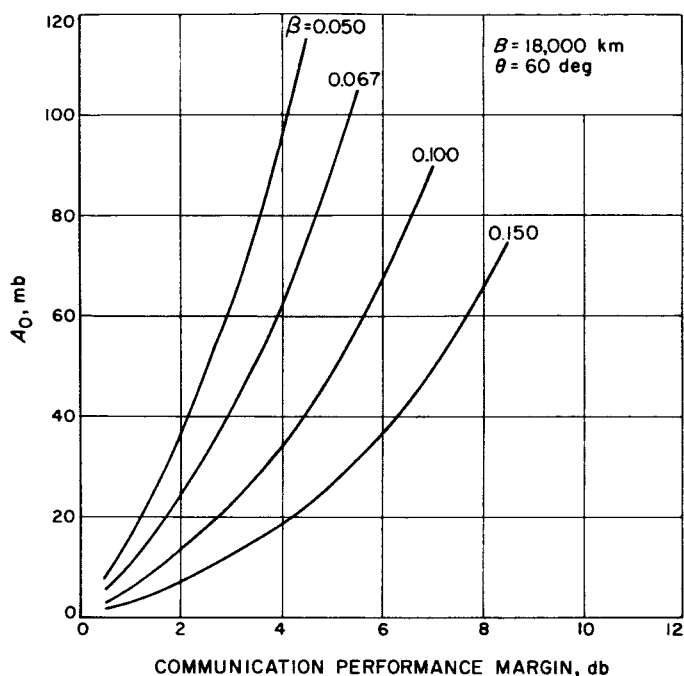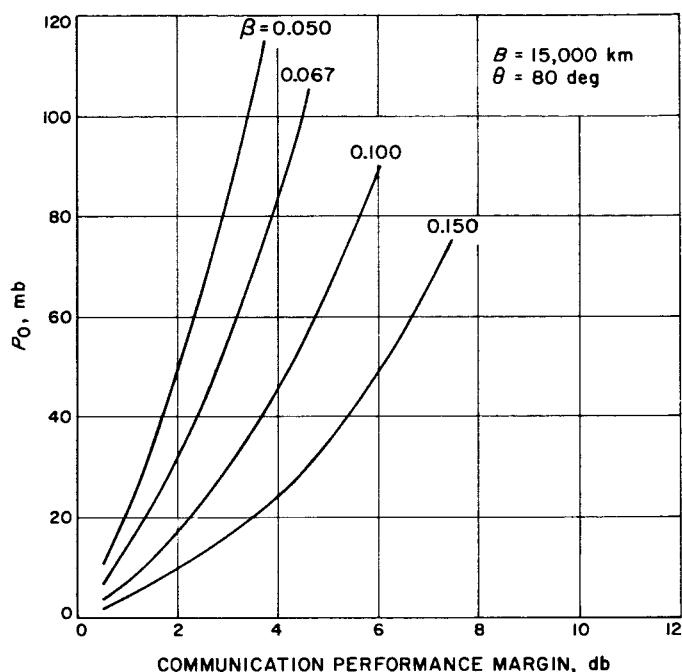
Fig. 56. Maximum measurable pressure vs. communications performance margin, trajectory 4, 1966-67

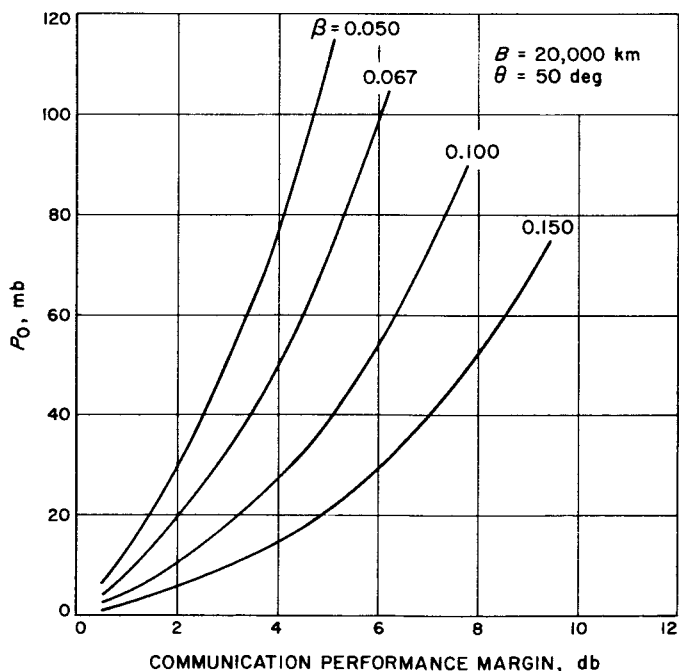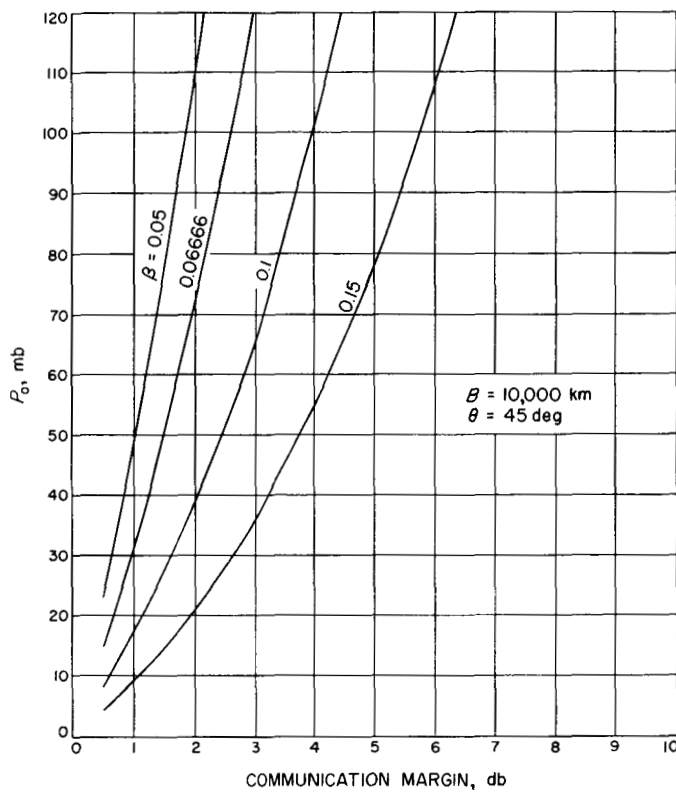**Fig. 57. Maximum measurable pressure vs. communications performance margin, trajectory 5, 1966-67**

Because of the combined effects of refraction and reflection, the analysis of the entire problem would be a formidable undertaking. In this discussion, it is only attempted to obtain a simplified understanding of the problem.

It is evident from Fig. 59 that the region in which spurious reflection might be a problem is confined by the spacecraft antenna pattern to a rather narrow range in the vicinity of the point of the trajectory at which the Earth-probe-near limb angle is zero. Geometrically, no reflection to the Earth is possible after the probe is physically occulted by the planet, but because of bending due to refraction, the range of reflection can be extended somewhat beyond the point of physical occultation. In any case, it is here assumed that the resulting reflection occurs at a very shallow angle and can be approximated by the geometry in Fig. 59.

First, let the assumption be made that the planet is a sphere, and the reflection is specular, with a reflection coefficient K. Then considering a narrow beam element

of angle $\Delta\eta$ arriving from the probe, the length, Δs, subtended by the beam element at the surface of the planet is approximately

$$\Delta s \cong \frac{R_A \, \Delta\eta}{\sin \Psi} \qquad (32)$$

The angle $\Delta\theta$ subtended at the center of the planet by the length Δs is then

$$\Delta\theta = \frac{\Delta s}{r_0} = \frac{R_A \, \Delta\eta}{r_0 \sin \Psi} \qquad (33)$$

The difference in angle of reflection between the extreme rays of the beam element is given by twice the angle $\Delta\theta$, and, therefore, the reflected beam has an angular width of approximately

$$\Delta\phi = \Delta\eta + 2\Delta\theta$$
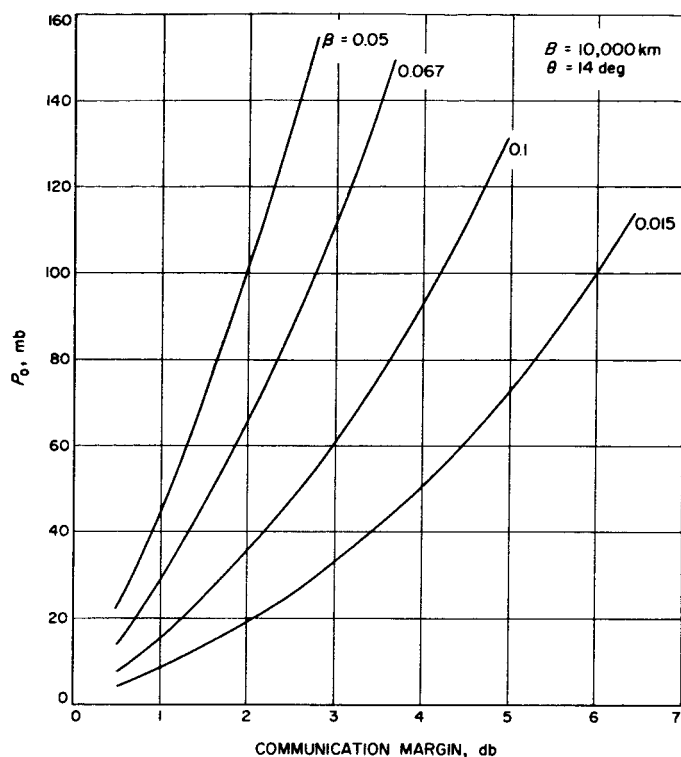
$$= \Delta\eta \left(1 + \frac{2R_A}{r_0 \sin \Psi} \right) \qquad (34)$$

Fig. 58. Maximum measurable pressure vs. communications performance margin, trajectory 6, 1966-67

Fig. 59. Geometry of multipath reflection

reflecting surface is also far from being smooth, and it is this assumption that is probably most inaccurate. Quite possibly, there may be surface features on Mars that would reflect portions of the signal from the probe with less attenuation than that computed above. However, there is no way to properly investigate this problem.

C. Other Problem Areas

In addition to the problems that were discussed in previous sections, certain other areas must be investigated before the feasibility of the occultation experiment can be firmly established. Among these problem areas are the following.

1. Diffraction

Because of the diffraction in the Martian atmosphere, the wave received at the DSN will be the sum of many waves which have traversed a family of paths through the atmosphere. Diffraction theory shows that the altitude difference between the extremes of the various paths is, to a good approximation, $(X\lambda)^{1/2}$, where X is the distance from the spacecraft to planet, and λ is the wavelength. At a range of 30,000 km, and with a 12-cm wavelength, this range of altitudes is about 2 km. The result of this is that the occultation experiment, rather than scanning the atmosphere with an infinitely good resolution scans it with a resolution of roughly 2 km. Since this is considerably less than any plausible scale height, no significant degradation of the final results is caused. Furthermore, because X enters only as the square root, the situation changes slowly with the range actually achieved at occultation.

2. Nonhomogeneous Atmosphere

There will be some scattering of the radiation due to inhomogeneities in the atmosphere (tropospheric scatter).

The attenuation caused by the reflection is then given by the following expression

$$A_r = \frac{1}{\kappa}\left(1 + \frac{2R_A}{r_0 \sin \Psi}\right) \tag{35}$$

Assuming, for example, that

$$R_A = 30,000 \text{ km}$$

$$r_0 = 3,415 \text{ km}$$

$$\Psi = 6 \text{ deg}$$

$$\kappa = 0.5$$

The attenuation of the reflected signal is found to be $A_r \cong 330$ or $10 \log A_r = 25.2$ db.

Based on the simplified analysis, it appears that reflection should not be a problem, at least if specular reflection from a spherical planet is assumed. The reflection in the actual case is, of course, not specular, but if diffuse reflection is assumed, the scattering effect is even greater and the reflected signals should be even weaker, in addition to being out-of-phase with one another. The
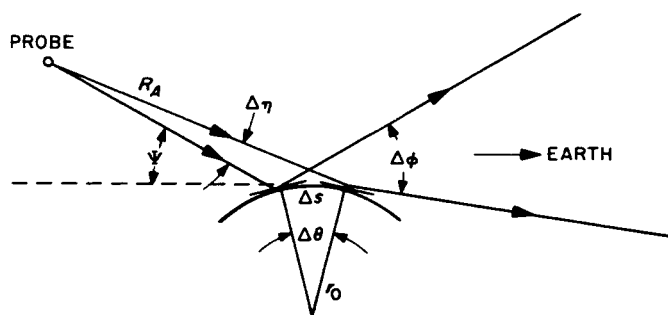
However, at the short wavelength used, and with the low mass of the atmosphere, these will clearly cause undetectable effects. This has already been verified by terrestrial radio telescopes.

3. Signal Reacquisition

No problem can be expected to arise in the area of DSN reacquisition after occultation provided that the doppler frequency can be predicted to within 50 cps and the rate of change of the doppler frequency is less than 10 cps^2.

Since orbit determination can predict the velocity of the spacecraft after occultation to a much greater accuracy than is required, and the rate of frequency change never exceeds 10 cps^2, no problem is foreseen in rapidly reacquiring two-way lock after occultation. It is even possible that two-way lock could be reestablished in time to secure useful data on the emerging side, and all attempts will be made to do so.

4. Ionospheric Effects

Any ionosphere that might exist around Mars would also have an effect on the 2300-Mc signal from the spacecraft, because of the refracting effect of an electrically charged medium.

For previously postulated denser models of the Martian atmosphere the ionospheric effect was assumed to be negligible. However, the newly formulated model atmospheres having much lower surface pressures may lead to ionosphere models in which the electron density is sufficient to cause an effect on the signal comparable to that caused by the neutral atmosphere.

Most probably this would not mask the atmospheric effect, because the ionospheric effect would occur at higher altitudes, where the electron densities are maximal. However, if ionospheric effects were very large, they could conceivably reduce the accuracy with which atmospheric parameters could be determined.

APPENDIX A

REFRACTION EFFECTS

The geometry is shown diagrammatically in Fig. A-1. In the absence of the planet, the path of the radio wave (considered a ray) would be the straight line *bde*. Due to refraction by the planetary atmosphere, the ray may take some other path *ace*. The difference in the path lengths
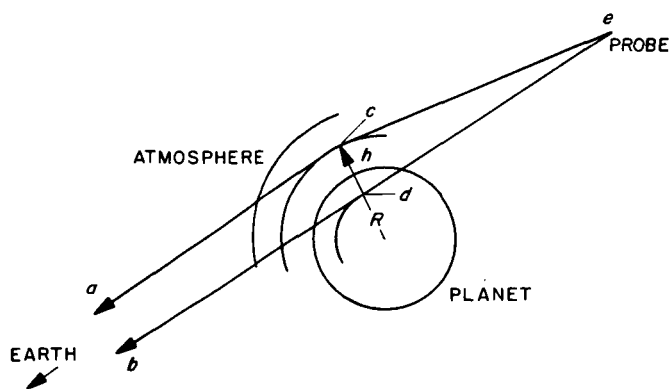
Fig. A-1. Refraction geometry

of their rates of change can be estimated accurately using a doppler tracking system and appropriate equations of motion for the spacecraft (at *e*). The path length difference may be computed by making the following assumptions:

1. The planet is spherical, with a spherically layered atmosphere in which the refractivity varies only with the height above the surface

2. The path of the ray takes the shortest time route, and this path is the solution of the two-dimensional problem (planar).

To examine the path of light ray, start at the point of closest approach to the planet, in Fig. A-2.

Define the index of refraction n as

$$n = c/v$$
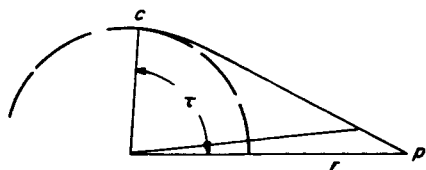
Fig. A-2. Definition of refraction angle

c = speed of light in vacuum

v = speed of light in planet atmosphere at a given point, p.

τ = angle to point p from closest approach point c

The problem reduces to finding the curve Γ for which the travel time, T_t is a minimum, i.e.,

$$T_t = \int^{\Gamma} \frac{ds}{v} = \text{minimum} \tag{A-1}$$

Using polar coordinates [because $n = n\,(r)$ only] we have

$$ds^2 = (r\,d\tau)^2 + (dr)^2 \tag{A-2}$$

$$T_t = \int_{r_i}^{\bar{r}} \frac{n}{c} \left[r^2 \left(\frac{d\tau}{dr} \right)^2 + 1 \, dr \right]^{1/2} \tag{A-3}$$

where r_i and $\bar{r}$ are specified limits. From the calculus of variations, the differential equation (Euler–Lagrange) for the extremum of $\int_{r_0}^{\bar{r}} f\,(r, \tau)\,dr$ is

$$\frac{\partial f}{\partial \tau} - \frac{d}{dr} \frac{\partial f}{\partial \dot{\tau}} = 0 \tag{A-4}$$

where

$$\dot{\tau} = \frac{d\tau}{dr}$$

Applying this formula yields

$$\frac{d}{dr} \left\{ n \left[r^2 \left(\frac{d\tau}{dr} \right)^2 + 1 \right]^{-1/2} r^2 \frac{d\tau}{dr} \right\} = 0 \tag{A-5}$$

Integrating once, and using C_1 to represent the constant of integration of the above equation, then

$$\frac{d\tau}{dr} = \frac{C_1}{r\,(n^2\,r^2 - C_1^2)^{1/2}} \tag{A-6}$$

The end conditions are: at $r = r_i$, $n_i = n\,(r_i)$ the slope is zero, or $d\tau/dr = \infty$; then

$$C_1 = n_i\,r_i \tag{A-7}$$

and the equation to be integrated is

$$\tau\,(\bar{r}) = \int_{r_i}^{\bar{r}} \frac{r_i\,n_i\,dr}{r\,(r^2\,n^2 - r_i^2\,n_i^2)^{1/2}} \tag{A-8}$$

To find the total bending (that over 90 deg), a change of variables is made. Let

$$u = rn \tag{A-9}$$

then

$$u\,(r_i) = u_i$$

$$\bar{u} = Rn\,(R)$$

$$du = (rn' + n)\,dr$$

$$n' = \frac{dn}{dr}$$

and

$$\tau = \int_{u_i}^{\bar{u}} \frac{n\,u_i\,du}{u\,(u^2 - u_i^2)^{1/2}\,(rn' + n)}$$

$$= u_i \int_{u_i}^{\bar{u}} \frac{du}{u\,(u^2 - u_i^2)^{1/2}} \left(\frac{1 - \dfrac{rn'}{n}}{1 + \dfrac{rn'}{n}} \right) \tag{A-10}$$

Integrating the first term:

$$\tau = \frac{\pi}{2} - u_i \int_{u_i}^{\bar{u}} \frac{1}{u\,(u^2 - u_i^2)^{1/2}} \frac{rn'}{(n + rn')}\,du \tag{A-11}$$

now the total bending (from infinity to closest approach) is defined

$$\epsilon \equiv - u_i \int_{u_i}^{\infty} \frac{rn'}{(n + rn')} \frac{du}{u\,(u^2 - u_i^2)^{1/2}} \tag{A-12}$$

The total angle ϵ, through which a ray is bent while passing through the atmosphere at a "closest approach" distance R, is then seen to be

$$\epsilon = - 2\,n\,(R)\,R \int_{R}^{\infty} \frac{n'\,(r)\,dr}{n\,(r)\,[n^2\,r^2 - n^2\,(R)\,R^2]^{1/2}} \tag{A-13}$$

Since $n(r)$ is assumed to be of the form

$$n(r) = (n_0 - 1) e^{-\beta(r-r_0)} + 1 \qquad \text{(A-14)}$$

then

$$n'(r) = -\beta(n_0 - 1) e^{-\beta(r-r_0)} \qquad \text{(A-15)}$$

Since, as a good approximation,

$$n \approx 1$$

and

$$n - 1 \ll 1$$

Eq. (A-13) can be approximated by

$$\epsilon \cong 2 \times 10^{-6} N_s \beta R e^{\beta r_0} \int_R^\infty \frac{e^{-\beta r}}{(r^2 - R^2)^{1/2}} dr \qquad \text{(A-16)}$$

letting $t = r - R$

$$\epsilon \cong 2 \times 10^{-6} r \beta N_s e^{-\beta h} \int_0^\infty \frac{e^{-\beta t}}{(t^2 + 2Rt)^{1/2}} dt \qquad \text{(A-17)}$$

The integral in Eq. (A-17) can be found in Laplace transform tables (Ref. 5) and Eq. (A-17) becomes

$$\epsilon \cong 2 \times 10^{-6} N_s e^{-\beta h} R\beta e^{\beta R} K_0(\beta R) \qquad \text{(A-18)}$$

but, from Ref. 6,

$$e^x K_0(x) = \left(\frac{\pi}{2x}\right)\left[1 - \frac{1}{8x} + \frac{9}{21(8x)^2} - \cdots + \right] \qquad \text{(A-19)}$$

and, for large values of x

$$e^x K_0(x) \cong \left(\frac{\pi}{2x}\right)^{1/2}$$

Hence, the angle ϵ can be approximated by

$$\epsilon \cong 2 \times 10^{-6} N_s e^{-\beta h} \beta \left(\frac{\pi R}{2\beta}\right)^{1/2} \qquad \text{(A-20)}$$

The retardation effect can now be derived as follows. In Fig. A-3 the geometry of the situation is shown schematically. The solid line represents a ray passing through the atmosphere of a planet of radius r_0 at a closest-approach distance of R.
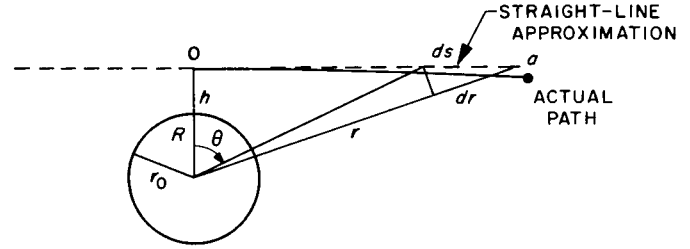

Fig. A-3. Geometry for computing retardation effects

The total time for the ray to travel from point 0 to some point a is given by

$$\tau = \frac{1}{c} \int_0^a n \, ds \qquad \text{(A-21)}$$

where c is the velocity of light and n is the index of refraction.

Thus, the measured range from point 0 to point a is

$$R_e = c\tau = \int_0^a n \, ds \qquad \text{(A-22)}$$

while the true distance is given by

$$R_0 = \int_0^a ds \qquad \text{(A-23)}$$

the difference, caused by the medium of nonunity refractive index is then

$$\Delta R = \int_0^a n \, ds - R_0 \qquad \text{(A-24)}$$

$$\cong \int_0^a (n - 1) \, ds$$

Since the increase in the length of path due to bending is a second-order effect in relation to the retardation, the integration in Eq. (A-24) can be approximated by integrating along the straight-line path (dotted line in Fig. A-3). This approximation is quite good for Mars, as the total bending amounts to only about 1 mrad.

From Fig. A-3

$$\cos \theta = \frac{R}{r} \qquad \text{(A-25)}$$

and

$$\sin \theta = \left[1 - \left(\frac{R}{r} \right)^2 \right]^{1/2}$$

and since

$$\frac{dr}{ds} \cong \cos(90 \deg - \theta) = \left[1 - \left(\frac{R}{r} \right)^2 \right]^{1/2} \quad \text{(A-26)}$$

hence

$$ds = \frac{dr}{\left[1 - \left(\frac{R}{r} \right)^2 \right]^{1/2}} \quad \text{(A-27)}$$

Now, if the refractivity of a medium is defined as

$$N(r) = 10^6 \left[n(r) - 1 \right] \quad \text{(A-28)}$$

then, again assuming an exponential atmosphere, the refractivity can be expressed as

$$N(r) = N_s e^{-\beta h}; \quad h = r - r_0 \quad \text{(A-29)}$$

where

N_s = refractivity at surface of planet

β = reciprocal of scale height

r_0 = radius of planet

Using Eq. (A-24), (A-28), and (A-29) the total retardation effect is given by

$$\Delta R = 2 \times 10^{-6} N_s \int_R^\infty \frac{e^{-\beta(r - r_0)}}{\left[1 - \left(\frac{R}{r} \right)^2 \right]^{1/2}} dr \quad \text{(A-30)}$$

letting $r = R + t$

$$\Delta R = 2 \times 10^{-6} N_s e^{-\beta(R - r_0)} \int_0^\infty \frac{(R + t) e^{-\beta t}}{(2Rt + t^2)^{1/2}} dt \quad \text{(A-31)}$$

The integral in Eq. (A-31), a Laplace transform (Ref. 5, p. 136), yields the following

$$\Delta R = 2 \times 10^{-6} N_s e^{-\beta h} R e^{\beta R} K_1(\beta R) \quad \text{(A-32)}$$

where $K_1(x)$ is a modified Bessel function which can be expressed asymptotically (Ref. 6, p. 202) by

$$e^x K_1(x) = \left(\frac{\pi}{2x} \right)^{1/2} \left[1 + \frac{3}{8x} - \frac{15}{21(8x)^2} + \cdots - \right] \quad \text{(A-33)}$$

Since βR is of the order of 200 for Mars, the approximation can be made that

$$e^{\beta R} K_1(\beta R) \cong \left(\frac{\pi}{2\beta R} \right)^{1/2} \quad \text{(A-34)}$$

and hence,

$$\Delta R = 2 \times 10^{-6} N_s e^{-\beta h} \left(\frac{\pi R}{2\beta} \right)^{1/2} \quad \text{(A-35)}$$

Equation (A-35) can be used to compute the retardation effect when the surface refractivity N_s and inverse scale height β are assumed to be known.

To compute the contribution of this effect to the change in doppler velocity it is necessary to obtain the derivative with respect to h. Thus

$$\frac{d}{dh} \Delta R(h) = 2 \times 10^{-6} N(h) \left[- \beta \left(\frac{\pi R}{2\beta} \right)^{1/2} + \frac{1}{2} \left(\frac{\pi}{2\beta R} \right)^{1/2} \right]$$

$$= \Delta R(h) \left(- \beta + \frac{1}{2R} \right) \quad \text{(A-36)}$$

Referring back to Eq. (A-20), it is seen that

$$\epsilon(h) \cong \beta \Delta R(h) \quad \text{(A-37)}$$

and

$$\frac{d}{dh} \epsilon(h) = \beta \frac{d}{dh} \Delta R(h) = \epsilon(h) \left(- \beta + \frac{1}{2R} \right) \quad \text{(A-38)}$$

APPENDIX B

DIFFERENTIAL REFRACTION

The geometry governing the differential refraction phenomenon is shown in Fig. B-1. Although the illustration shows the effect on the probe-to-Earth signal, the influence on the signal from the Earth to the probe is exactly analogous.

A beam element diverging with an angle η leaves the probe and subtends a width Δh in the planetary atmosphere. Due to differential refraction, the beam element leaving the atmosphere has an angle of divergence in the Earth–planet–probe plane of

$$\theta = \eta + \Delta \epsilon \qquad \text{(B-1)}$$

but

$$\Delta \epsilon = \epsilon' (h) \, \Delta h \qquad \text{(B-2)}$$

where

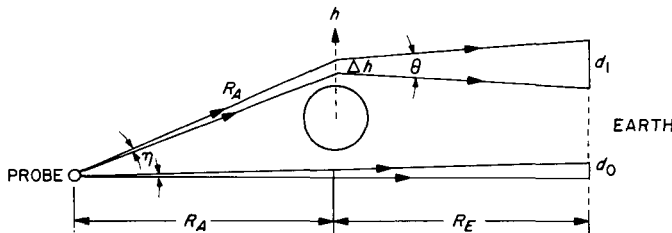$$\epsilon' (h) = - \frac{d}{dh} \epsilon (h)$$

Fig. B-1. Differential refraction geometry

and

$$\Delta h = R_A \, \eta \qquad \text{(B-3)}$$

and therefore

$$\theta = \eta \left[1 + R_A \, \epsilon' (h) \right] \qquad \text{(B-4)}$$

Then, the width subtended by the beam element at the Earth is approximately

$$d_1 = \Delta h - R_E \, \theta = \left[R_A + R_E + R_A \, R_E \, \epsilon' (h) \right] \eta \quad \text{(B-5)}$$

Without the differential refraction effect, the beam element would arrive at the Earth with a width

$$d_0 = (R_A + R_E) \, \eta \qquad \text{(B-6)}$$

For a narrow beam, the effect is one-dimensional, and the attenuation of the signal due to differential refraction is proportional to the ratio of the widths subtended by the beam elements and is given by

$$A (h) = 1 + \frac{R_A \, R_E}{R_A + R_E} \epsilon' (h) \qquad \text{(B-7)}$$

Because near occultation the distance R_E is much larger than R_A, Eq. (B-7) can be approximated by

$$A (h) \cong 1 + R_A \, \epsilon' (h) \qquad \text{(B-8)}$$

NOMENCLATURE

A attenuation

A_r reflected-signal attenuation

B miss parameter magnitude

c velocity of light

f frequency

h altitude of ray above surface of planet

H scale height

K_0 modified Bessel function of 0th order

K_1 modified Bessel function of 1st order

n index of refraction

N refractivity

N_s refractivity at surface of planet

N_0 refractivity at point where last data taken

P_0 surface pressure

r_0 radius of planet

R distance from center of planet to closest approach point of a ray

R_A probe-to-Mars distance

R_E Earth-to-Mars distance

R_s Mars-to-spacecraft distance along Earth-Mars line

S incoming asymptote direction

t time

T absolute temperature

T_c count time in seconds

T_t travel time

$\mathbf{T}$ vector normal to $\mathbf{S}$ lying in ecliptic plane

$V_{x_{pT}}$ velocity of probe relative to Mars in a plane normal to the Earth-Mars direction

β reciprocal of scale height

ϵ angle of refractive bending

κ reflection coefficient

λ wavelength

ρ range

$\dot{\rho}$ range rate

σ standard deviation

τ time of occultation

REFERENCES

1. Kaplan, L. D., Munch, G., and Spinrad, H., "An Analysis of the Spectrum of Mars," *Astrophysical Journal*, Vol. 139, No. 1, January 1964.

2. Kuiper, G. P. (to be published as "University of Arizona Lunar and Planetary Communications No. 31 and 32") 1964.

3. *Space Programs Summary No. 37-16*, Vol. III, p. 30, Jet Propulsion Laboratory, July 31, 1962.

4. *Space Programs Summary No. 37-16*, Vol. III, p. 33, Jet Propulsion Laboratory, July 31, 1962.

5. Bateman Manuscript Project, *Higher Transcendental Functions*, California Institute of Technology, ed. by A. Erdelyi, Vol. 1, McGraw-Hill Book Co., Inc., New York, 1953.

6. Watson, G. N., *A Treatise on the Theory of Bessel Functions*, Cambridge University Press, New York, 1958.

ACKNOWLEDGMENT